FACULTY OF MECHATRONICS,
INFORMATICS AND INTERDISCIPLINARY
STUDIES TUL

Master thesis

DNA origami nanostructures for applications in medicine

Study programme: N0719A270001 – Nanotechnology
Study branch: N0719A270001NA – Nanotechnology
Author: **Bc. Agnes Zerolová**
Supervisor: Mgr. Jaroslav Kočišek, Ph.D.
Consultant: Leo Albert Sala, Ph.D.

Liberec 2023

FAKULTA MECHATRONIKY,
INFORMATIKY A MEZIOBOROVÝCH
STUDIÍ TUL

Diplomová práce

DNA origami nanostruktury pro medicínské aplikace

Studijní program: N0719A270001 – Nanotechnologie
Studijní obor: N0719A270001NA – Nanotechnologie
Autor práce: **Bc. Agnes Zerolová**
Vedoucí práce: Mgr. Jaroslav Kočišek, Ph.D.
Konzultant: Leo Albert Sala, Ph.D.

Liberec 2023

FAKULTA MECHATRONIKY,
INFORMATIKY A MEZIOBOROVÝCH
STUDIÍ TUL

Zadání diplomové práce

DNA origami nanostructures for applications in medicine

Jméno a příjmení:	**Bc. Agnes Zerolová**
Osobní číslo:	M21000194
Studijní program:	N0719A270001 Nanotechnologie
Zadávající katedra:	Katedra chemie
Akademický rok:	2022/2023

Zásady pro vypracování:

1. Studentka uskuteční rešerši problematiky, kde se zaměří na vlastnosti DNA a různé přístupy přípravy DNA nanostruktur, současný stav v oblasti aplikací DNA nanostruktur k cílenému dodávání léčiv a jako biosenzorů za použití cisplatiny jako chemo a chemo-radioterapeutika.
2. Připraví 2D a 3D origami nanostruktury modifikované léčivem.
3. Zapojí se do evaluace biologického účinku DNA v in vitro experimentech.
4. Připraví 2D DNA biosenzor na bázi DNA origami rámečku a otestuje jeho funkcionalitu.

Část projektu se uskuteční ve spolupráci s ÚFCH J. Heyrovského AV ČR v Praze, část může být realizována na spolupracujících pracovištích v Potsdam (DE) a Biofyzikálním ústavu AV ČR v Brně.

Student

1. Will carry out literature research with focus on the properties of DNA and different approaches to DNA nanostructure preparation, cisplatin as chemo and chemo-radiotherapeutic agent and the current state of art in DNA nanostructures for targeted drug delivery and for biosensors.
2. Will prepare 2D and 3D origami nanostructures loaded with cisplatin.
3. Will participate in the in vitro evaluation of the biological effects of the prepared nanostructures.
4. Prepare a single molecule biosensor based on a DNA origami frame and tests its functionality.

Rozsah grafických prací:	dle potřeby dokumentace
Rozsah pracovní zprávy:	50 stran
Forma zpracování práce:	tištěná/elektronická
Jazyk práce:	Angličtina

Seznam odborné literatury:

1. ENDO, M., ed., 2022. *DNA origami: structures, technology, and applications*. *Wiley*. ISBN 9781119682547.
2. SALA, L., PERECKO, T., MESTEK, O., PINKAS, D., HOMOLA, T., KOČIŠEK, J. 2022. *Cisplatin-Cross-Linked DNA Origami Nanostructures for Drug Delivery Applications*. *ACS Applied Nano Materials*. **5**(9), 13267-13275. ISSN 2574-0970. Dostupné z doi: 10.1021/acsanm.2c02976.
3. SALA, L., LYSHCHUK, H., ŠÁCHOVÁ, J., CHVÁTIL, D., KOČIŠEK, J. 2022. *Different Mechanisms of DNA Radiosensitization by 8-Bromoadenosine and 2'-Deoxy-2'-fluorocytidine Observed on DNA Origami Nanoframe Supports*. *The Journal of Physical Chemistry Letters*. **13**(17), 3922-3928. ISSN 1948-7185. Dostupné z doi: 10.1021/acs.jpclett.2c00584.
4. RAVEENDRAN, M., a spol., 2020. *Rational design of DNA nanostructures for single molecule biosensing*. *Nature Communications*. ISSN 2041-1723. Dostupné z doi: 10.1038/s41467-020-18132-1.

Vedoucí práce:	Mgr. Jaroslav Kočišek, Ph.D. Ústav fyzikální chemie J. Heyrovského AV ČR
Konzultant práce:	Leo Albert Sala, Ph.D. Ústav fyzikální chemie J. Heyrovského AV ČR
Datum zadání práce:	10. října 2022
Předpokládaný termín odevzdání:	22. května 2023

L.S.

prof. Ing. Zdeněk Plíva, Ph.D.
děkan

prof. Ing. Josef Šedlbauer, Ph.D.
vedoucí katedry

V Liberci dne 20. října 2022

Prohlášení

Prohlašuji, že svou diplomovou práci jsem vypracovala samostatně jako původní dílo s použitím uvedené literatury a na základě konzultací s vedoucím mé diplomové práce a konzultantem.

Jsem si vědoma toho, že na mou diplomovou práci se plně vztahuje zákon č. 121/2000 Sb., o právu autorském, zejména § 60 – školní dílo.

Beru na vědomí, že Technická univerzita v Liberci nezasahuje do mých autorských práv užitím mé diplomové práce pro vnitřní potřebu Technické univerzity v Liberci.

Užiji-li diplomovou práci nebo poskytnu-li licenci k jejímu využití, jsem si vědoma povinnosti informovat o této skutečnosti Technickou univerzitu v Liberci; v tomto případě má Technická univerzita v Liberci právo ode mne požadovat úhradu nákladů, které vynaložila na vytvoření díla, až do jejich skutečné výše.

Současně čestně prohlašuji, že text elektronické podoby práce vložený do IS/STAG se shoduje s textem tištěné podoby práce.

Beru na vědomí, že má diplomová práce bude zveřejněna Technickou univerzitou v Liberci v souladu s § 47b zákona č. 111/1998 Sb., o vysokých školách a o změně a doplnění dalších zákonů (zákon o vysokých školách), ve znění pozdějších předpisů.

Jsem si vědoma následků, které podle zákona o vysokých školách mohou vyplývat z porušení tohoto prohlášení.

22. května 2023 Bc. Agnes Zerolová

DNA origami nanostruktury pro medicínské aplikace

Abstrakt

Tato diplomová práce se zabývá využitím DNA origami v medicíně a navazuje na moji bakalářskou práci *DNA origami nanostruktury pro studium radiosenzitizačního efektu nanočástic*. V teoretické části jsou popsány různé postupy přípravy dvourozměrných a trojrozměrných DNA origami nanostruktur. Rovněž jsou zmíněny hlavní oblasti jejich využití v medicíně. Hlavním výsledkem experimentální části je příprava a depozice 3D DNA origami nanostruktur ve tvaru nanobloku o velikosti $\sim$ 12 nm x 12 nm x 22 nm a jejich modifikace cisplatinou a rutheniovým komplexem pro další experimenty. Dále také příprava a depozice 2D DNA origami nanostruktur ve tvaru trojúhelníku se stranou $\sim$ 120 nm a nanorámečku o velikosti $\sim$ 80 nm x 90 nm funkcionalizovaný G-quadruplexem pro další experimenty. Kromě optimalizace přípravy nanostruktur byly také provedeny vlastní experimenty studující cytotoxicitu modifikovaných DNA origami nanostruktur léčivy a poškození těchto nanostruktur laserovým zářením.

Klíčová slova: DNA, DNA origami, DNA nanotechnologie, rakovina, doprava léčiv, cisplatina, ruthenium, samoskládání, cytotoxicita, senzor, stabilita, laser

DNA origami nanostructures for applications in medicine

Abstract

The present master's thesis is focused on the application of DNA origami in medicine. This thesis is a continuation of my bachelor's thesis *DNA origami nanostruktury pro studium radiosenzitizačního efektu nanočástic* (in Czech). The theoretical part of the work overviews the various approaches to the preparation of two-dimensional and three-dimensional DNA origami nanostructures. The main applications in medicine are also mentioned. The main result of the experimental part of the present thesis is the preparation and characterization of 3D DNA origami in the shape of a nanoblock with a size of ∼ 12 nm x 12 nm x 22 nm and their modification with cisplatin and ruthenium complex for further experiments. Other experimentally prepared nanostructures include triangular DNA origami with a side length ∼ 120 nm and nanoframe with a size of ∼ 80 nm x 90 nm functionalized with G-quadruplex for further experiments. In addition to the optimization of the preparation, further individual experiments were performed to study the cytotoxicity of drug-modified DNA origami nanostructures and the damage of triangular nanostructures under laser irradiation.

Keywords: DNA, DNA origami, DNA nanotechnology, cancer, drug delivery, cisplatin, ruthenium, self-assembly, cytotoxicity, sensor, stability, laser

Acknowledgements

First and foremost, I would like to thank my supervisor Mgr. Jaroslav Kočišek, Ph.D. for his unlimited advice and support during this whole process. Also, many thanks to L. A. Sala, Ph.D. for all the help and advice. Furthermore, I would like to thank Mgr. J. Pinkas, Ph.D. from the J. Heyrovský Institute of Physical Chemistry of the CAS, Mgr. D. Pinkas from the Institute of Molecular Genetics of the CAS and Mgr. T. Perečko, Ph.D. from the Institute of Biophysics of the CAS, without their help this work would not be possible. Last but not least, I would like to thank my family and friends for their unlimited support.

Contents

List of abbreviations

A	adenine
AFM	atomic force microscope
AGE	agarose gel electrophoresis
AuNPs	gold nanoparticles
C	cytosine
Cl^-	chlorine anion
CO_2	carbon dioxide
Cryo-TEM	cryogenic-transmission electron microscope
DDS	drug delivery system
DMEM	Dulbecco's modified Eagle medium
DNA	deoxyribonucleic acid
DNR	daunorubicin
DONs	DNA origami
DOX	doxorubicin
dsDNA	double-stranded DNA
EPR effect	enhanced permeability and retention effect
FaDu	human squamous cell carcinoma
FBS	fetal bovine serum
G	guanine
g	G-Force
GQ	G-quadruplex
HCl	hydrochloric acid
ICL	interstrand cross-links
ICP-MS	inductively coupled plasma mass spectrometry
K^+	potassium cation
KCl	potassium chloride
Mg^{2+}	magnesium(II) cation
$MgCl_2 \cdot 6H_2O$	magnesium chloride hexahydrate
nt	nucleotide
Pt	platinum
Pt^{2+}	platinum(II) cation
Ru	ruthenium
Ru^{2+}	ruthenium(II) cation
Ru^{3+}	ruthenium(III) cation
ROS	reactive oxygen species
Si	silicon
SPR	surface plasmon resonance
ssDNA	single-stranded DNA
T	thymine
TAE	tris-acetate-EDTA
TCA	trichloroacetic acid
TE	tris-EDTA
TEM	transmission electron microscope
tris	tris(hydroxymethyl)aminomethane
UV	ultraviolet light

1 Introduction

DNA origami nanostructures are emerging as an impressive new nanomaterial in many fields of science and technology. Due to the biocompatibility of DNA as a material and the flexibility of the DNA origami design, an intensely explored field of said materials is medicine. In the present thesis, I focused on fundamental studies towards the utilization of DNA nanostructures in two particular applications. The first application is drug delivery, the second one is biosensing. This thesis is a continuation of my bachelor's thesis [1].

Aiming to reach the goals set in the thesis topic description, I performed a series of experiments focused on loading the DNA origami nanostructures with anti-cancer agents, modification of DNA origami with G-quadruplexes for sensing applications, and further explored the stability and cytotoxicity of such DNA origami complexes.

The thesis consists of a theoretical part and an experimental part. The theoretical part explains the preparation of DNA origami nanostructures and their applications in medicine. Chapter 2.1 describes the preparation of two- and three-dimensional DNA origami nanostructures. Chapter 2.2 describes DNA origami in medical applications. Subsection 2.2.1 focuses on some anti-cancer drugs used in the field as well as in the present study. Subsection 2.2.2 overviews the state of the art in the use of DNA origami for cancer treatment. At the end of the theoretical part, subsection 2.2.3 describes possible ways to use DNA origami in sensing applications.

The experimental part begins in Chapter 3 with a detailed description of the experimental methodology and the materials used. Chapter 4 is dedicated to the results and discussion of my experiments. The main portion of the laboratory work focused on the loading of DNA origami nanostructures with a model for cross-linking chemotherapeutic agent cisplatin and intercalating agent $[Ru(bpy)_2dppz](PF_6)_2$, described in sections 4.1 and 4.3 and their cytotoxicity studies described in sections 4.2 and 4.4, respectively. A comparison of *in vitro* efficiency of these two agents is in section 4.5. The last two sections 4.6 and 4.7 describe my activities as part of a complex research work towards biosensing applications of DNA origami, which is undergoing at J. Heyrovský Institute of the CAS. Chapter 4.6 focuses on the stability of DNA origami nanostructures upon irradiation with light and chapter 4.7 on the modification of DNA origami frames with G-quadruplex strands.

2 Theoretical background

2.1 DNA origami

DNA strands can be self-assembled into predesigned shapes due to the strict complementarity between DNA bases as described by the Watson-Crick model [2][3]. DNA, DNA nanostructures (DNA origami, DNA nanothreds, etc.) and DNA-functionalized nanoparticles are biocompatible, biodegradable and have low cytotoxicity. Especially DNA structures and their nanoparticle heterostructures have been suggested for cancer treatment and offer many advantages over current clinically approved nanomedicines [4]. Antibody fragments, aptamers and affibodies have been linked to DNA nanostructures to provide (actively-targeted) drug delivery systems [5]. For drug delivery purposes, DNA nanostructures must be stable in a biological system. It has been demonstrated that the stability in biological media depends on the shape and structural design of the DNA nanostructures [4][6]. Another important factor is their interaction with nucleases that may induce nanostructure decomposition [7][8]. With the development of various new techniques, DNA nanotechnology has evolved into a multi-disciplinary field, facilitating the construction of various patterns with different components, which hold great potential for applications including bioimaging, drug delivery system (DDS), optical sensors, nanorobotics, nanoelectronics, etc. [3][9][10][11].

DNA nanotechnology is based on a proposal by Seeman (1982), who designed a cross-shaped DNA structure based on naturally-occurring DNA cross-overs called Holliday junctions (Fig. 2.1) [12]. Then Mao et al. expanded Seeman's cross structure with three-, four- and six-arm DNA tiles [13].

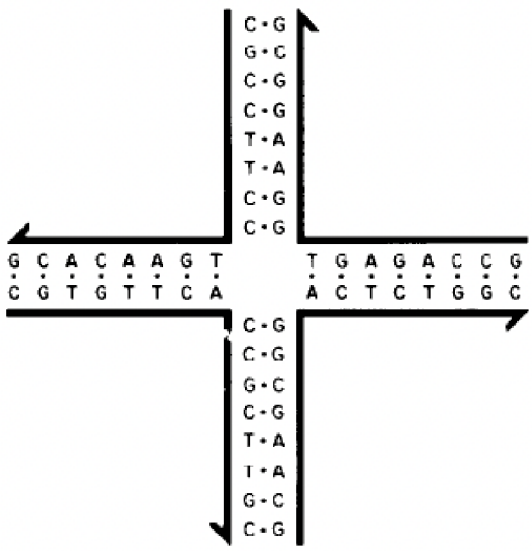

Figure 2.1: Scheme of a cross-shaped DNA structure by Seeman based on Holliday junctions [12].

In 2006, Rothemund clarified the methodology of folding DNA origami using single-stranded DNA (ssDNA). Rothemund constructed several 2D DNA origami shapes of $\sim$ 100 nm x 100 nm [14][15]. The DNA origami technique is based on the self-assembly of a long scaffold DNA strand into the desired shape using hundreds of oligonucleotide staples of 15 - 60 nt in length (short ssDNA strands/oligonucleotides) [11][16]. DNA origami is folded in one step as shown in Fig. 2.2A where the scaffold is mixed with oligonucleotide staples in TAE buffer with a high concentration of Mg^{2+} cations. This mixture is then heated to 90 °C. This leads to thermal denaturation of the DNA meant for easy access to the scaffold DNA bases for hybridization. The mixture is then cooled slowly to room temperature to kinetically assist the self-assembly process [17][18][19].

Based on Rothemund's method, different shapes of 2D DNA origami were gradually designed and synthesized [20]. A commonly used scaffold is the purified ssDNA M13mp18, which is 7249 nt in length [21][22][23]. Its disadvantage is its limited length and high probability of cleavage [13][24]. To solve this problem, long dsDNA or long ssDNA instead of M13mp18 was used [25][13]. Yan et al. used dsDNA to design square and triangular DNA origami [25]. While Fan et al. used long ssDNA to design a hierarchical pore structure [26]. Yen et al. proposed curved structures that provided the theoretical background for the construction of 3D DNA origami nanostructures [20]. It is also possible to create constructions of complex 2D geometric shapes with irregular boundaries [27]. Zhang et al. designed even more complex wireframe structures using a multi-arm junction [28].

The first attempt to create a 3D structure was made by Seeman et al. in 1991 [29]. Afterwards, Joyce et al. constructed DNA origami octahedron using long ssDNA paired with several staples [30]. 3D DNA origami can be prepared in two ways. The first is to fold 2D DNA origami and through complementary base pairing, form a 3D DNA origami nanostructure [31]. Komiyama et al. constructed a DNA origami cube based on this concept. The six 2D DNA origami planes were formed from M13mp18 and folded into the desired structure using staples [32]. The second is to form 3D DNA origami with curved surfaces by implementing crossover structures and guiding the surface formation [20]. Yan et al. designed a DNA origami hemisphere, vase, and spherical shape, and Liedl et al. designed a hollow rigid tetrahedral frame structure with a length of 75 nm by bottom-up assembly method [33][34].

In recent years, multilayer DNA origami nanostructures have been developed. These multilayer nanostructures are composed of a honeycomb or tetragonal lattice in helical arrangement [13]. Gothelf et al. designed a DNA origami hollow cubes formed by routing the scaffold to form a box. Multilayer DNA origami nanostructures can also be formed from 3D DNA origami [35][36][37]. Dietz et al. constructed a self-limiting ring oligomer DNA origami by assembling multilayer "V" shapes, which were then formed into a tubular shape [38].

Various software programs have been developed to design DNA origami [15]. The most commonly used program is caDNAno, which allows one to guide the scaffold to the desired shape and predict crossovers between any two staples or scaffold bases [39].

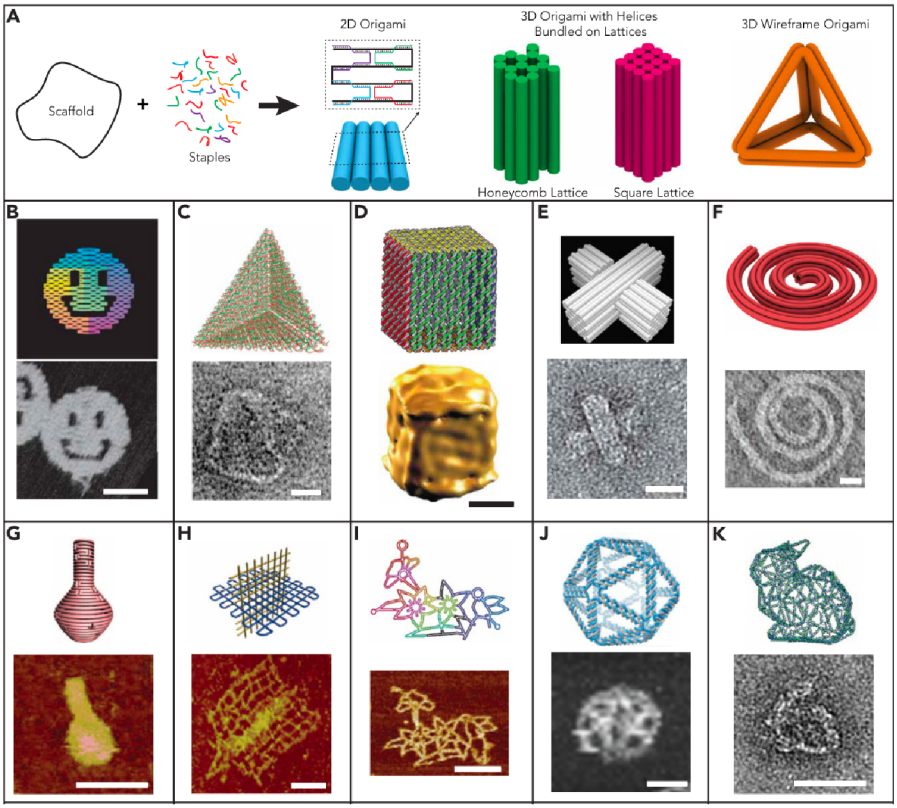

Figure 2.2: Overview of DNA origami nanostructures from the work of Wang et al., demonstrating the versatility of approach. a) Schematic illustration of DNA origami preparation by Rothemund, b) 2D DNA origami "smiley face", c) 3D DNA origami cube, d) 3D DNA origami hollow tetrahedron, e) 3D DNA origami slotted cross f) 3D DNA origami in spiral shape, g) 3D DNA origami in flask shape, h) 3D DNA origami gridiron, i) 2D DNA origami wireframe flower and bird, j) 3D DNA origami wireframe icosahedron, and k) 3D DNA origami wireframe rabbit [40].

2.2 Medical applications

2.2.1 Anti-cancer drugs

Doxorubicin

Doxorubicin (DOX) is the most well-known and widely administered cytotoxic drug for cancer treatment [41]. DOX belongs to the anthracycline antibiotics class. At room temperature it is a hygroscopic crystalline powder composed of orange-red thin needles [42].

In the early 1960s, two anthracyclines - doxorubicin and daunorubicin (DNR) - were successfully isolated from *Streptomyces peucetius*. Both drugs consist of aglyconic (hydrophobic) and sugar moieties (hydrophilic). The side chain of DOX terminates with a primary alcohol, whereas DNR terminates with a methyl group (Fig. 2.3) [42][43]. Daunorubicin was first discovered and used to treat acute leukemia and lymphomas. Although the treatment was successful, it was recognised that it could cause fatal cardiac toxicity. Consequently, researchers genetically modified *Streptomyces peucetius* to produce a drug that was later called DOX [44].

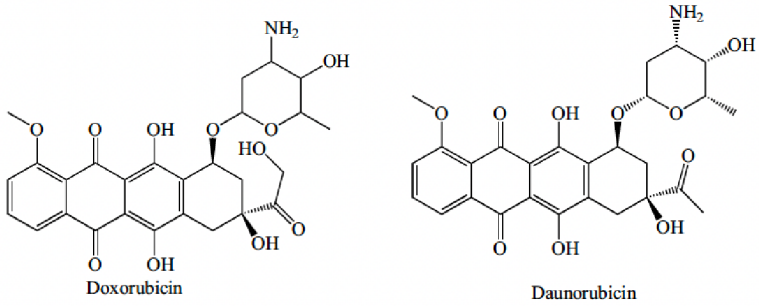

Figure 2.3: Chemical structures of doxorubicin and daunorubicin [45].

The exact mechanism of action of DOX is still under study, but it is known that DOX intercalates into DNA (Fig. 2.4), thereby inhibiting the biosynthesis of macromolecules [44]. It is believed that DNA scission occurs through the action of topoisomerase II or iron-catalyzed free radical formation [42]. DOX also produces ROS which break DNA bonds and degrade DNA, inhibiting mRNA transcription and ultimately leading to cell death [46].

In 2012, Denard et al. demonstrated that DOX induces cellular toxicity via a novel mechanism. This mechanism involves ceramide (a lipid molecule) synthesis followed by activation of a transcription factor CREB3L1 [47]. Tumour cells with elevated levels of CREB3L1 are more sensitive to DOX, while those with low levels are resistant [48].

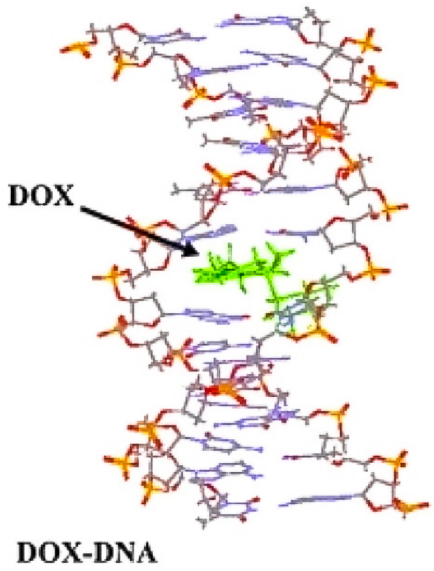

Figure 2.4: Scheme illustration of intercalated DOX into DNA [49].

Although DOX is an effective anti-cancer drug, it causes cardiotoxicity and also induces apoptosis and necrosis in healthy tissue [41][50]. Combination therapy or use of various materials (e.g. liposomes, metal nanoparticles, synthetic polymers, DNA origami, etc.) can facilitate the drug delivery, reduce drug resistance and reduce side effects [48][51].

Cisplatin

One of the main goals of the work was to modify the DNA origami by cisplatin. Cisplatin (CDDP, *Cis*-diamminedichloroplatinum(II)), a platinum (Pt) coordination complex has been clinically proven to be effective in the treatment of various types of cancer (e.g. lung, breast, ovarian, bladder, etc.) [52][53]. Cisplatin and its less toxic analog *cis*-diammine-1,1-cyclobutanedicarboxylatoplatinum(II) known as carboplatin are commonly used in clinical practice. Both of these compounds show the same spectrum of anti-tumour activity as sarcomas, germ cell tumours, carcinomas and lymphomas. Cisplatin is administered intravenously as a brief infusion with normal saline solutions for the treatment of solid malignancies [52][54].

At the room temperature, it is a white or deep yellow-orange crystalline powder. It is stable at room temperature and normal pressure, but may slowly transform to its *trans*-isomer overtime [53]. Cisplatin contains two ammine (NH_3) ligands and two labile chlorido (Cl) ligands in a *cis* configuration to each other that function as leaving groups (Fig. 2.5A) [55].

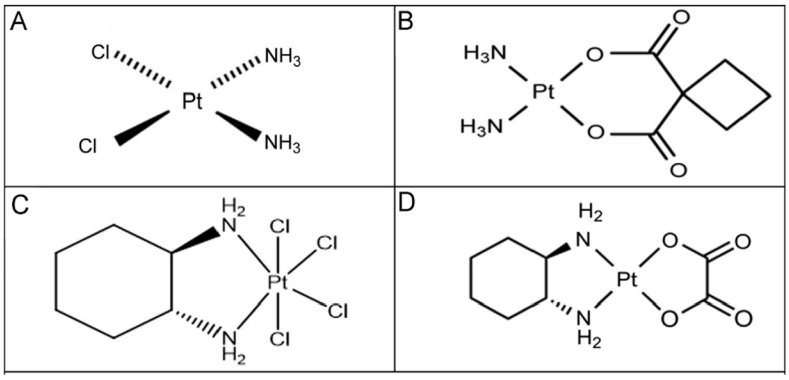

Figure 2.5: Chemical structures of selected platinum drugs. a) cisplatin, b) carboplatin, c) oxaliplatin, d) ormaplatin [53].

In 1844 M. Peyrone first synthesized cisplatin and A. Werner elucidated its chemical structure in the late 19^{th} century. Since the 1960's, Rosenberg's observations caused much interest in applying these coordination complexes of platinum, palladium and other noble metals in cancer treatment [53][56]. Due to drug resistance and side effects, there is an intense effort to develop new platinum compounds that are able to overcome the problems associated with chemotherapy using cisplatin and carboplatin. Unfortunately, finding analogous compounds to replace cisplatin and carboplatin has proved to be difficult [54][55].

The most common side effects of chemotherapy are nausea and vomiting. Cisplatin can also cause nephrotoxicity, hepatotoxicity, neurotoxicity and cardiotoxicity. Therefore, combination chemotherapy is preferred [52]. Combination chemotherapy leads to increased treatment effectiveness, synergism and reduced toxicity. In combination therapy, cisplatin is combined with another cancer drug such as carboplatin, oxaliplatin, ormaplatin or radiation [53]. Wang and co-workers examined the synergistic combination chemotherapy of DOX and cisplatin in breast cancer cells, the drugs were loaded to hyaluronic acid/chitosan-based nanoparticles. The results showed that both drugs exhibited a synergistic effect on cell apoptosis [57]. The study of Szturz et al. examined *in vivo* tests to detect the effect of high-dose and low-dose cisplatin in the chemoradiation of head and neck cancer. The results indicate a lack of evidence to suggest whether there is a significant difference in cell viability between the two dose regimes [58]. The study of Iwata et al. examined the biological effects of protons and X-ray irradiation combined with cisplatin. The study demonstrated no significant difference between X-ray and proton irradiation. The results show that high concentrations of cisplatin combined with proton therapy seemed to be more effective than X-ray therapy [59]. The platinum complexes mentioned above and others are currently in clinical trials around the world [53].

Modification of DNA by cisplatin

The primary action of cisplatin and platinum analogues is to interact with DNA in order to form DNA adducts, interfering with DNA replication and repair thus inducing cell apoptosis. The interaction between cisplatin and the DNA form covalent adducts with purine DNA bases. The cytotoxicity and toxicity effects of cisplatin are diverse and have been an area of interest to many oncologists and researchers [52][54].

DNA binding by metal ions can be divided into three categories (Fig. 2.6) [60].

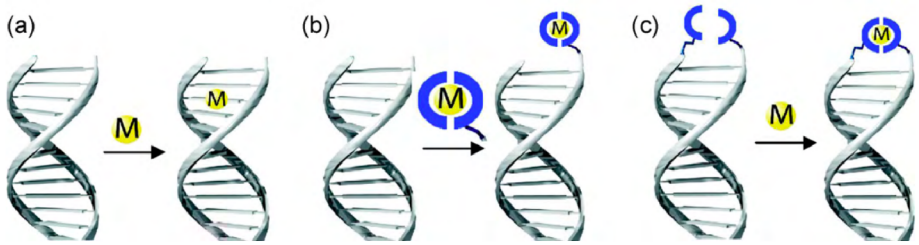

Figure 2.6: Schematic illustration of site-specific metal binding to unmodified DNA. a) metal binding to unmodified DNA, b) metal complexes binding to DNA, c) metal binding to ligand-modified DNA [60].

The first approach is direct binding to DNA [60]. This approach, used also in the present work, is equivalent to the cisplatin mechanism of action in living tissue. Once the drug is administered, in the cytosol where the concentration of chlorides is low, cisplatin goes through a process known as aquation (Fig. 2.7) [61]. This process immediately displaces from cisplatin one or two chloride atoms and replaces them with H_2O molecules [53]. Cisplatin thus becomes highly reactive and binds to various biomolecules inside the cell [61]. The hydrolyzed product has significant importance as an electrophile due to its ability to engage in reactions with nucleophiles, such as nitrogen donor atoms on nucleic acids and sulfhydryl groups on proteins [52]. In the first step of DNA binding, cisplatin binds to the nucleophilic N7 atoms of purine bases [61]. For B-DNA (DNA in a B-conformation), these sites are located in the major groove of DNA [54]. This binding leads to the modification of DNA in cancer cells [52]. The monofunctional adducts resemble bifunctional lesions, such as intrastrand and interstrand cross-links (ICL) [54]. ICLs are highly toxic, because they are blocking DNA transcription and replication. The most common adducts formed by cisplatin in linear DNA are 1,2-intrastrand GG or 1,2-intrastrand GA and 1,2-interstrand GG ICLs [54]. This process is very important in DNA transcription and replication. When the cell cycle is arrested, more time is allowed for DNA repair mechanisms. If the repair is disrupted or the DNA is damaged, then the cells undergo apoptosis. Studies have demonstrated that the changes in DNA such as 1,2-intrastrand GG, 1,3-intrastrand adducts, interstrand adducts and other nonfunctional adducts have been closely linked to toxicity of the drug [52].

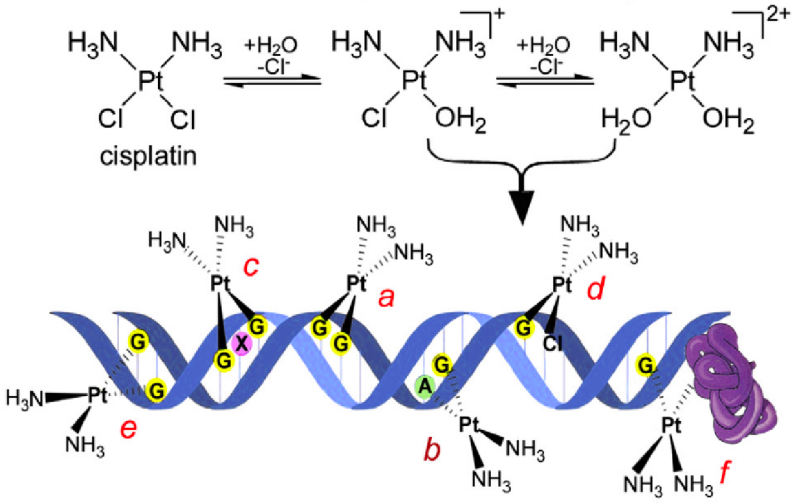

Figure 2.7: Schematic illustration of cisplatin hydration or aquation followed by hydrolysis when binding to DNA and the possible DNA adducts formed in cell environment. a) intrastrand cross-linking two neighbouring guanines, b) intrastrand cross-linking neighbouring adenine and guanine, c) 1,3 intrastrand cross-linking, d) monoadduct, e) interstrand cross-link, f) DNA–Pt–protein cross-link [62].

The second approach involves the synthesis of metal complexes that bind to DNA. This approach combines a phosphoramidite derivative of a metal complex with DNA during standard automated DNA synthesis. Metal complexes must be inert, resistant to oxidation and resistant to acids and bases [60].

The third approach involves the attachment of a ligand through a modified base- or phosphate backbone, followed by the binding of the metal to the ligand-modified DNA. It may be advantageous to first attach a ligand to DNA and then attach the metal. Another advantage of binding a ligand to DNA is compatibility with DNA synthesis methods. Ligands can be easily linked into any position of a DNA sequence using their phosphoramidite derivatives. In addition, the metal can bind selectively to ligands. To coordinate metal ions, ligands are incorporated into DNA either by synthesis of artificial bases or by attachment of the ligand to the DNA backbone by chemical means [60].

Ruthenium complex

Due to cisplatin side effects, suitable platinum-based alternatives are designed [63]. In addition to cisplatin, metal-based therapeutic drugs also include ruthenium complexes (Fig. 2.8) [64]. Compared to cisplatin, ruthenium complexes show promising cytotoxic effects (mimicking the binding of iron to biomolecules) and are able to overcome drug resistance [65][66]. Over the last few years, their properties have been studied for use in drug delivery applications. Three ruthenium complexes, NAMI-A, KP1019 and KP1339, are currently in clinical trials [64].

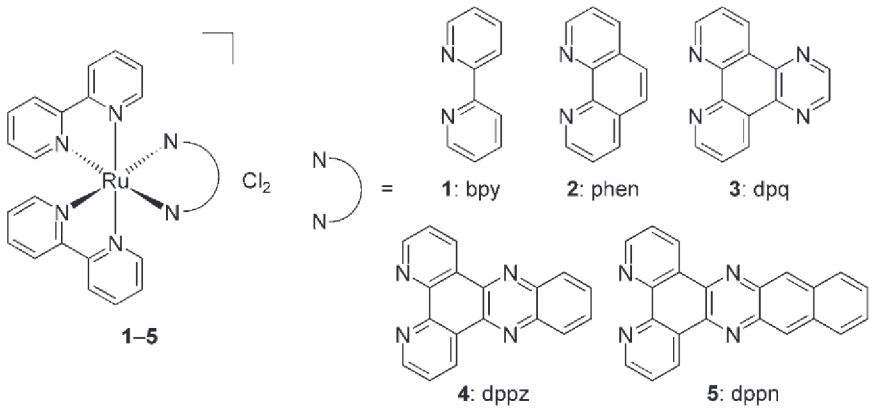

Figure 2.8: Chemical structures of ruthenium complexes [65].

The ruthenium ion is stable only in two oxidation states, Ru^{2+} and Ru^{3+}, in the physiological environment. The reduced state is more reactive [67]. The activity of ruthenium-based compounds depends on the oxidation state and the ligands, which cleave CGA, TGA and CGT triplets [66][68]. Compared to cisplatin, ruthenium complexes intercalate into DNA similarly as DOX via the DNA intercalating ligands [68]. For this master's thesis I used the $[Ru(bpy)_2dppz](PF_6)_2$ compound (Fig. 2.9). This ruthenium complex is luminescent in aqueous solution after intercalation with DNA [68].

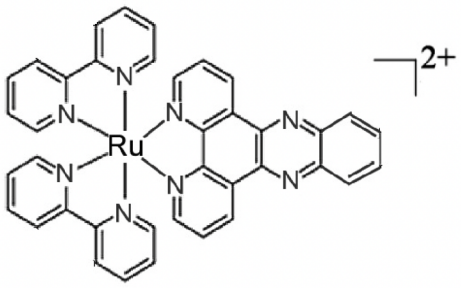

Figure 2.9: Chemical structure of the ruthenium complex I used, $[Ru(bpy)_2dppz](PF_6)_2$ [62].

Ru^{2+} polypyridyl complexes are suitable photosensitizers because photoactivation can cause DNA cross-linking, cytotoxic compounds release from molecular carriers or activation of prodrugs by ligand displacement [67][68]. These complexes are stable in the dark and after exposure to visible light become cytotoxic [69]. The excited photosensitizer molecules then activate oxygen or biomolecules to generate ROS, causing cell apoptosis [67]. In addition to studying Ru-complexes for chemotherapy, they have also been studied for use in photodynamic therapy (PDT) and photoactivated chemotherapy (PACT) [67][68]. In PDT treatment, photosensitiser molecules are administered either locally or intravenously and the target tissue is irradiated with light of a specific wavelength after the prodrug has been internalized into the tumour cells. In PACT treatment, light irradiation induces activation of the internalized drug [67]. Selective drug delivery to tumour cells and its activation by irradiation is a promising approach to enhance tumour cell cytotoxicity and thereby minimize side effects [67].

2.2.2 DNA origami for cancer treatment

Cancer is among the top causes of morbidity and mortality in the world with millions of new cases reported every year [3]. When an atypical cell division occurs, there is a possibility that it will corrupt other cells in the vicinity. This is commonly referred to as cancer [52]. Chemotherapy is a standard cancer treatment using cytotoxic anti-cancer drugs [70]. The main goal of chemotherapeutic drugs is to induce apoptosis or senescence of tumour cells [52][61]. Traditional chemotherapeutics are nonspecifically distributed by the blood circulation to the tumour and healthy tissue, which can cause severe systemic toxicity with undesirable side effects. A new direction in cancer treatment is focused on drug delivery systems (DDS) to avoid side effects during cancer treatment [4]. The development of effective and safe cytotoxic drug vehicles to target tumour cells is one of the major challenges in modern pharmacology [3].

Over the past few decades, various organic and inorganic nanomaterials have been used to create nanostructures to facilitate DDS [6]. It is important to ensure that these nanomaterials are safe, biocompatible and effective for *in vivo* drug

delivery. Researchers discovered that nanoparticle-based drug delivery systems have a great future for medicine [3]. After more than 15 years of DNA origami research, DNA nanotechnology has recently been explored for DDS [71]. DNA origami-based DDS have demonstrated passive targeting EPR (extended permeability and retention) effects. This effect arises from the increased permeability of tumour vasculature, which allows better penetration of relatively large particles (10 - 300 nm) such as nanoparticles, liposomes, micelles or proteins into the interstitial space of the tumour, where drug accumulation can occur [70][72]. On the other side the EPR effect is not as enhanced as other nanoparticle-based DDS [73]. Therefore, several active targeting strategies were developed for DONs, including folic acid or antibody modified DONs [74][75][76].

For *in vitro* and *in vivo* studies, denaturing agents and environmental stress (temperature, pH, and enzymatic cleavage during preparation) may cause damage to the DONs [71][77]. Stability in the biological environment is important [71]. It has been shown that the cellular uptake efficiency of DONs is influenced by shape, size, and type [78]. Also, the electrical charge on the surface of DONs can affect their behaviour in the bloodstream and their excretion from the body. With the polymer coating, stability in the bloodstream is enhanced [71]. For applications, further properties of DONs are being explored, such as immunogenicity, biocompatibility, biodistribution, selective targeting, degradation, etc. (Fig 2.10) [78]. However, it should be mentioned that the field of DNA origami research for DDS is still in the preclinical stages of testing [78].

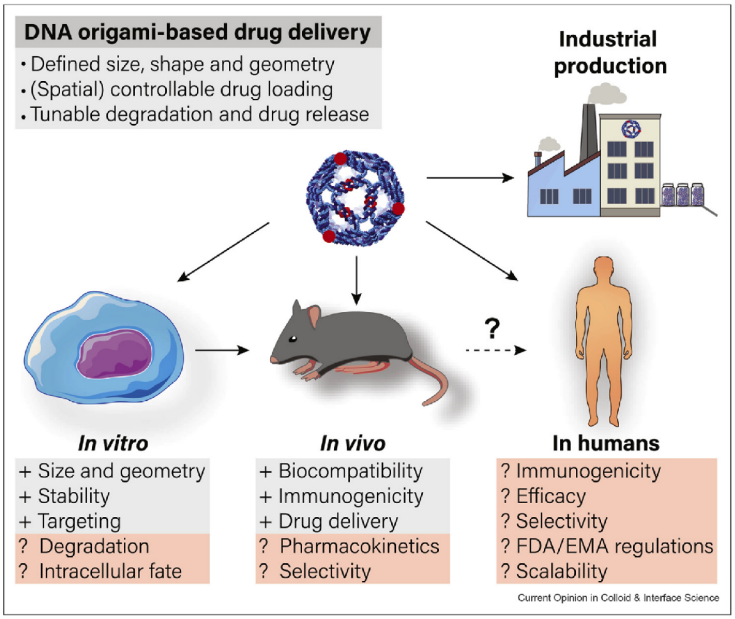

Figure 2.10: DNA origami applications for drug delivery, current status (grey) and underexplored areas (orange) [78].

For the present work is particularly important the study of Zhong [79]. The study focused on the preparation of 3D DNA origami in three different sizes (6H x 73nt, 4 x 4 x 64nt and 6 x 6 x 64nt, corresponding to 6 nm x 5.4 nm x 24 nm, 8 nm x 8 nm x 22 nm and 12 nm x 12 nm x 22 nm, respectively) and determining the toxicity when they are loaded with the cisplatin prodrug. The preparation of DNA origami nanoblocks loaded with a cisplatin prodrug using oligonucleotide staples is shown in Fig. 2.11 [79].

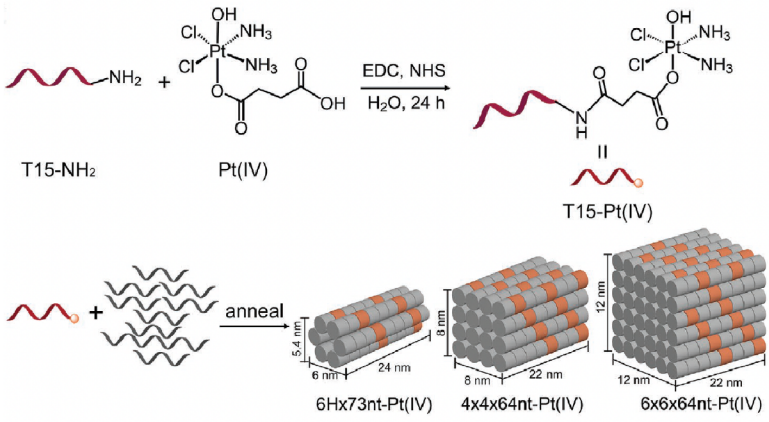

Figure 2.11: Schematic illustration of preparation 3D DNA origami nanoblocks loaded with a Pt(IV) cisplatin prodrug [79].

Xenograft cancer cell mice were injected intravenously with pure DONs. Tumour accumulation of DONs was analyzed. As shown in Fig. 2.12, fluorescence images of organs and tumour were taken after 6, 12 and 24 hrs of injection. As shown in Fig. 2.13, fluorescence intensities of organs were compared by quantitative analysis. The 6 x 6 x 64nt structure showed high tumour fluorescence signal even at 24 hrs, while the smaller 4 x 4 x 64nt structure lasted only 12 hrs. Meanwhile, Zhong et al. found that all three structures showed significant accumulation in the kidneys compared with the other organs. This indicates that the DONs were excreted through the kidneys and could serve as safe carriers for drug delivery applications [79].

The publications of Zhong et al. and Sala et al. demonstrated that pure DNA origami are non-cytotoxic and that these nanostructures are potentially suitable for DDS applications. Moreover, the cytotoxicity of cisplatin-loaded DNA origami increases with increasing cisplatin concentration [77][79].

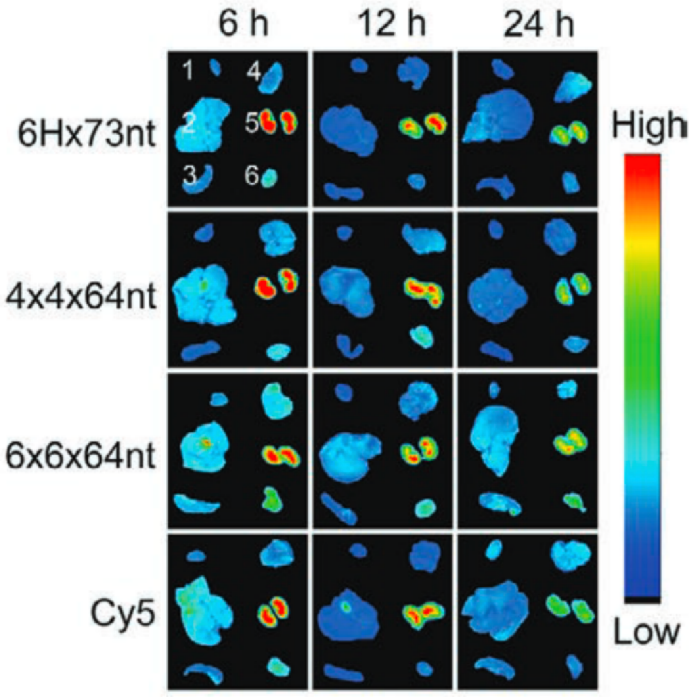

Figure 2.12: Fluorescence imaging of organs (1 - heart, 2 - liver, 3 - spleen, 4 - lung, 5 - kidney, and tumour (6)) of injected mice. Cy5 is a Cy5-labeled ssDNA used as control [79].

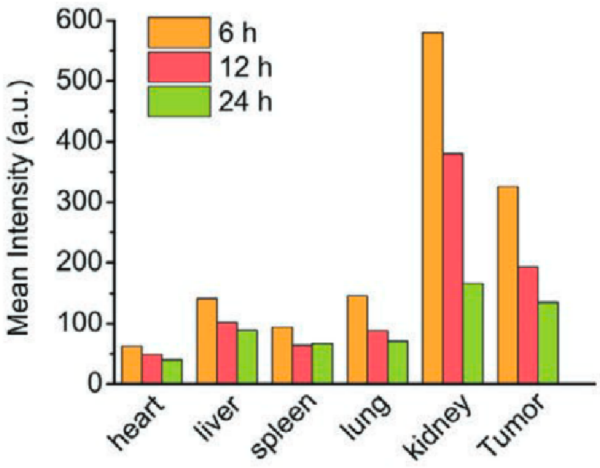

Figure 2.13: Fluorescence intensities of organs and tumour of mice injected with 6 x 6 x 64nt DNA origami nanoblocks [79].

2.2.3 Biosensors

For medical applications, DNA origami can also be used for sensing due to their stability and their ability to be functionalized on their surfaces [80]. In particular, 2D DNA origami nanostructures become attractive materials for sensing because it is easy to bind various functional groups to it [40][80]. By functionalizing the surface, DNA origami can obtain new properties and biological functions [81][82]. Utilization of DNA origami in sensing applications, therefore requires detailed studies of stability and biocompatibility of the designed nanostructures [83].

In modern healthcare, fast and inexpensive detection of biomarkers is increasingly desirable for early diagnosis. Common biosensors can only detect one type of biomarker. The creation of biosensors capable of detecting multiple biomarkers in small sample volume was proposed. These can be nucleic acids, peptides, proteins, molecules, cancer cells, viruses, etc. [83][84].

Yan et al. were the first who tried DNA origami as a sensor for *in-singulo* mRNA detection [85]. Detection of miRNA (MicroRNA) is required for therapeutic use and cancer treatment [83][86].

Another interesting sensor design was demonstrated by Nie and co-workers. It is based on DNA tetrahedron probes (DTPs) functionalized with AuNPs and with a sensitive SPR (surface plasmon resonance) sensor that was integrated onto gold films. When an analyte was detected in the sample, the SPR signal increased through electronic coupling along with the expanding size of the AuNPs, as shown in Fig. 2.14 [87][88].

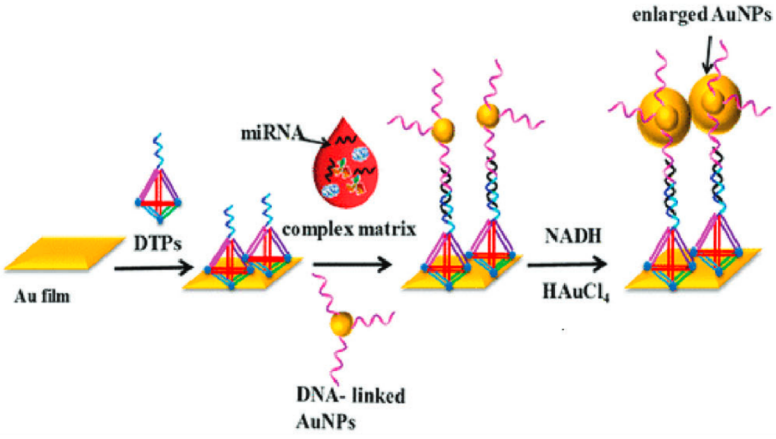

Figure 2.14: Schematic illustration of miRNA sensing by DTPs [88].

Walter et al. prepared a "traffic light" DNA origami sensor for ATP (adenosine triphosphate) sensing which fluoresces green, but after detecting ATP it switches colour to red, as shown in Fig. 2.15 [89].

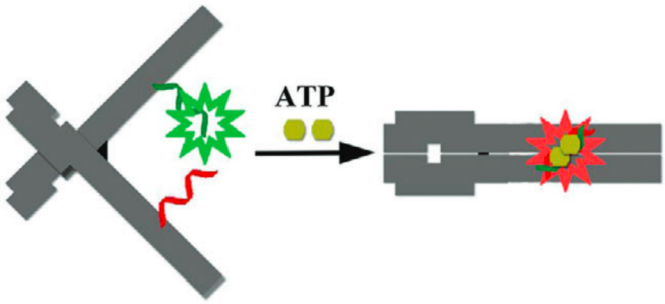

Figure 2.15: Schematic illustration of ATP sensing by "traffic light" DNA origami [83].

Proteins serve as the basic unit for many cellular activities, therefore protein sensing is also essential for diagnosis [83][90]. Biosensors can be used only for proteins that interact directly with DNA (proteins with target aptamers, enzymes, etc.) or with low-modified oligonucleotides (fluorescein, biotin, etc.) [91]. Enzyme-linked immunosorbent assays (ELISA), western blotting, SPR, fluorescence biosensors and others are used to detect protein [83]. Zhou et al. demonstrated the use of DNA origami tetrahedron for methyltransferase by fluorescence sensing [83].

My work on the topic was motivated by attempts to use G-quadruplexes (GQs), a single dsDNA strand composed of four guanine-rich domains that can align to form a tetrad structure, in biosensing applications [80]. GQs can be classified according to topology - antiparallel or parallel, as shown in Fig. 2.16 [92].

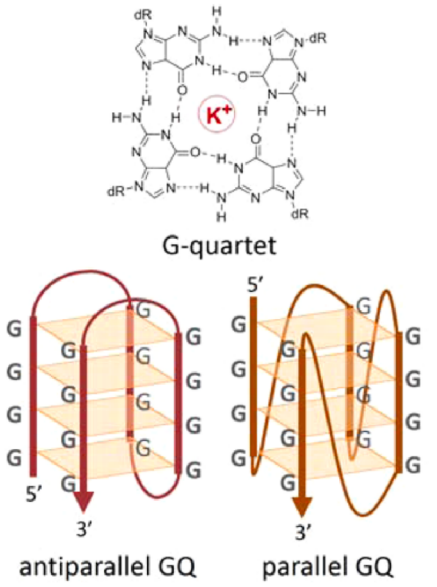

Figure 2.16: Schematic illustration of antiparallel and parallel G-quadruplex [92].

Endo et al. created a "DNA frame" (80 nm × 90 nm) with an empty rectangular area (40 nm × 40 nm). Inside the empty area, four connecting sites were introduced to hybridize two different dsDNA [93]. To form a GQ, a metal cation (commonly in the form of K^+) is needed [92]. Figure 2.17 shows that in the presence of K^+, the two G-rich strands formed an X-shape forming the G-quadruplex tetrad in the middle of the frame [94]. Such change of the shape from parallel to crossed structure is an example of a simple cationic sensor. Instead of the change in shape, which will be hard to evaluate in real life applications, the G-quadruplexes can be modified by fluorescent molecules for detection. Examples have been provided in several previous studies motivating the present work [95][96].

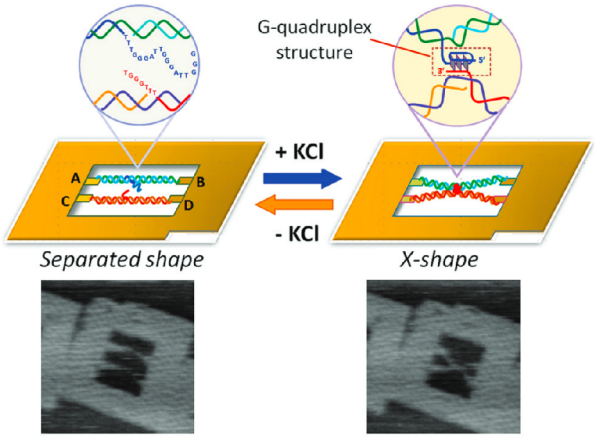

Figure 2.17: Schematic illustration of G-quadruplex formation in the presence of KCl and the corresponding AFM images (175 nm x 175 nm) [94].

3 Methodology

3.1 Materials

3.1.1 Chemicals

- oligonucleotide staples (Metabion International AG, Germany)
- 6 x 6 x 64nt staple mix (Metabion International AG, Germany)
- ethanol (Lach-Ner s.r.o., Czechia)
- 10x TAE buffer (Sigma-Aldrich, Germany)
- $MgCl_2 \cdot 6H_2O$ (Sigma-Aldrich, Germany)
- HCl (Sigma-Aldrich, Germany)
- Trizma (tris) base, Primary Standard and Buffer, $\geq$ 99.9% (titration), crystalline (Sigma-Aldrich, Germany)
- cisplatin (Sigma-Aldrich, Germany)
- Ru-complex $[Ru(bpy)_2dppz](PF_6)_2$ (synthesized by Mgr. J. Pinkas, Ph.D. from J. Heyrovský Institute of the CAS, Czechia)
- DMEM 1X, high glucose (41966-029, 500 mL) (Thermofisher, USA)
- FBS (10270-106, 500 mL) (Thermofisher, USA)
- Penicilin/Streptomycin (Thermofisher, USA)
- MTT (thiazolyl blue) (Duchefa Biochemie, Netherlands)
- Triton X-100 lysis buffer (Sigma-Aldrich, Germany)
- uranyl acetate (Sigma-Aldrich, Germany)
- SYBR Green I (10,000 $\times$ in DMSO) (Sigma-Aldrich, Germany)
- agarose gel (Serva Electrophoresis, Germany)
- 6x loading dye (Thermofisher, USA)

- acetic acid, 99.8% (Penta s.r.o., Czechia)
- trichloroacetic acid (Sigma-Aldrich, Germany)
- sulforhodamine B sodium salt (SRB) (Sigma-Aldrich, Germany)

3.1.2 Solutions

These are aqueous solutions unless otherwise stated.

- 10x TAE buffer with 125 mM $MgCl_2$
  1.14 g of $MgCl_2 \cdot 6H_2O$ is topped up with 10x TAE buffer to a volume 45 mL
- 1x TAE buffer
  4.5 mL of 10x TAE buffer is topped up with Milli-Q H_2O to a volume 45 mL
- 1x TAE buffer with 12.5 mM $MgCl_2$
  1.14 g of $MgCl_2 \cdot 6H_2O$ is topped up with 1x TAE buffer to a volume 45 mL
- 5x TE buffer supplemented with 400 mM $MgCl_2$
  0.3 g tris is mixed with 0.073 g of 5 mM EDTA and 4.1 g of 400 mM $MgCl_2 \cdot 6H_2O$ and is topped up with Milli-Q H_2O to a volume 50 mL, pH adjustment, 1M HCl is added slowly (pH = 8)
- 0.5x TAE buffer
  100 mL 10x TAE buffer is topped up with Milli-Q H_2O to a volume 2 L
- H_2O with 100 µM $MgCl_2$ buffer
  10 µL of 0.5 M $MgCl_2$ stock solution topped up with Milli-Q H_2O to a volume of 50 mL
- growth medium
  composition: DMEM 1X with high glucose, 10% FBS and 1% Penicilin/Streptomycin
- 2% agarose gel
  0,7 g of agarose is dissolved in 35 mL of 0.5x TAE with 6 mM $MgCl_2$
- Ru-complex in buffer
  3.7 mg of Ru-complex is dissolved in 15 mL of 0.5x TE buffer with 40 mM $MgCl_2$
- 0.5x TE buffer supplemented with 40 mM $MgCl_2$
  5 mL of 5x TE buffer supplemented with 400 mM $MgCl_2$ is topped up with Milli-Q H_2O to a volume 50 mL

3.1.3 Cells

- FaDu cell line (ATCC, USA)

3.2 Instrumentation equipments

- thermal cycler - modified CH-100 heating block (BioSan, USA)
- centrifuge - Minispin (Eppendorf, Germany)
- plasma cleaner - RPS40 (Roplass, Czechia)
- AFM - Scanning Probe Microscope Bruker Dimension Icon (ICON-SPM) (Bruker, USA)
- Vortexer - BV1000 vortex mixer (Benchmark, USA)
- Microplate reader - Infinite M200 Pro spectrophotometer (Tecan, Austria)
- UV-Vis spectrophotometer - NanoDrop™ One Microvolume (Thermofisher, USA)
- electrophoresis kit (Cleaver Scientific, UK)
- TEM - Jeol JEM-F200 (Jeol, Japan)
- Conventional TEM - Jeol JEM-1400 (Jeol, Japan)
- optical microscope (Zeiss, Germany)
- ICP-MS - NexION 350D with high-efficiency plasma torch (Perkin-Elmer, USA)
- micropipettes - P-2.5, 10, 20, 100, 1000 (Eppendorf, Germany)
- centrifugal filters - 100 kDa MWCO Amicon filters (Sigma-Aldrich, Germany)
- plastic tubes of volume 0.5, 1.5 and 2 mL (Eppendorf, Germany)
- 96-well plate - cell culture plate (Thermofisher, USA)
- silicon wafer (MicroChemicals GmbH and Siegert Wafer, both Germany)
- carbon-coated copper TEM grids (Electron Microscopy Sciences, USA)
- copper TEM grids (Electron Microscopy Sciences, USA)
- UV transilluminator (Vilber, France)
- NT-230 with OPO - laser beam with optical parametric oscillator (EKSPLA, Lithuania)
- analytical balance
- laboratory glassware

3.3 Software

- Gwyddion 2.59 (GNU license) for visualizing AFM results
- Origin Pro for data processing
- MS Excel for data processing
- ImageJ 2.9.0 (GNU license) for editing TEM results

3.4 Sample preparation

3.4.1 2D DNA origami preparation

Triangles

Preparation of DNA origami triangles is based on the original work of P. Rothemund [14]. Single-stranded M13mp18 viral DNA (6 µL, 100 nM) composed of 7249 bases was mixed with an excess concentration of 208 oligonucleotide staples (30 µL, 480 nM), in 1x TAE buffer with 12.5 mM $MgCl_2$ and additional Milli-Q H_2O to reach a final volume of 100 µL. Solution was then heated to 90 °C and slowly cooled down to 10 °C at a rate of -0.7 °C/min on thermal cycler (costumized using arduino platform to precisely regulate and program temperature ramping). The DNA origami solution was then filtered through 100 kDa MWCO Amicon filters three times to remove excess staples with 1x TAE buffer with 12.5 mM $MgCl_2$ to a final volume of $\sim$ 500 µL and centrifuged at 4000 g for 4 min each cycle. During each cycle, 1x TAE buffer with 12.5 mM $MgCl_2$ was added to a final volume of $\sim$ 500 µL. Subsequently, the filter with DNA origami was flipped into a clean tube and centrifuged at 4000 g for 2 min to recover the filtered DNA solution.

Frames

Preparation of DNA origami frames is based on the original work of Endo et al. and Sala et al. [93][97]. Single-stranded M13mp18 viral DNA (6 µL, 100 nM) composed of 7249 bases was mixed with an excess concentration of 208 oligonucleotide staples (30 µL, 480 nM), in 1x TAE buffer with 12.5 mM $MgCl_2$ (and with 50 mM KCl for G-quadruplex-containing nanoframes) and additional Milli-Q H_2O to reach a final volume of 100 µL. 1 µL each of the duplex strands (500 nM) to be placed in the frame aperture was also added in this step for experiments requiring them. Solution was then heated to 90 °C and slowly cooled down to 10 °C at a rate of -0.7 °C/min on thermal cycler (costumized using arduino platform to precisely regulate and program temperature ramping). The DNA origami solution was then filtered through 100 kDa MWCO Amicon filters three times to remove excess staples with 1x TAE buffer with 12.5 mM $MgCl_2$ (and with 50 mM KCl for G-quadruplex-containing nanoframes) to a final volume of $\sim$ 500 µL and centrifuged

at 4000 g for 4 min each cycle. During each cycle, the corresponding buffer was added to a final volume of ∼ 500 µL. Subsequently, the filter with DNA origami was flipped into a clean tube and centrifuged at 4000 g for 2 min to recover the filtered sample.

3.4.2 3D DNA origami preparation

Nanoblocks

Preparation of DNA origami nanoblocks is based on the original work of Zhong et al. [79]. The 6 x 6 x 64nt DNA origami nanoblocks were designed to be 12 x 12 x 22 nm. The 6x6x64nt staple mix (900 µl, 0.68 µM), all DNA strands, were mixed to a final concentration of 200 nM per strand in 100 µL of 0.5x TE buffer (pH = 8) supplemented with 40 mM $MgCl_2$. The resulting solution was then heated to 95 °C for 20 min then slowly cooled down to 65 °C for 1 h, 65 to 53 °C for 18 hrs, 53 to 44 °C for 12 hrs and then a slow linear cooling to room temperature for 18 hrs. The DON solution solution was filtered three times with H_2O with 100 µM $MgCl_2$ to a final volume of ∼ 500 µl and centrifuged at 4000 g for 4 min each cycle. During each cycle, H_2O with 100 µM $MgCl_2$ was added to a final volume of ∼ 500 µl. Subsequently, the filter with DNA origami was flipped into a clean tube and centrifuged at 4000 g for 2 min. DNA concentration was measured using the NanoDrop™ One Microvolume UV-Vis spectrophotometer and subsequently adjusted with the appropriate buffer as needed.

3.5 Drug loading to DNA origami nanoblocks

3.5.1 Cisplatin

Cisplatin loading procedures for DNA origami nanoblocks were adapted from the procedure used by Sala et al., where they loaded cisplatin to 2D DNA origami nanotriangles [77]. Pure DNA origami nanoblocks are mixed with corresponding volume of cisplatin stock solution (4.5 mM) to meet the desired cisplatin-nanoblock concentration ratio. After the loading time (16 hrs), the cisplatin-loaded DNA origami nanoblocks solution was filtered three times with H_2O with 100 µM $MgCl_2$ to a final volume of ∼ 500 µL and centrifuged at 4000 g for 4 min each cycle. During each cycle, H_2O with 100 µM $MgCl_2$ was added to a final volume of ∼ 500 µL. Subsequently, the filter with DNA origami nanoblocks was flipped into a clean tube and centrifuged at 4000 g for 2 min. DNA concentration was estimated using the NanoDrop™ One Microvolume UV-Vis Spectrophotometer and subsequently adjusted with the appropriate buffer as needed. Cisplatin concentration in the filtered sample was estimated from the Pt content measured using ICP-MS.

3.5.2 Ruthenium complex

The stock solution of the Ru-complex (250 µM Ru-complex in 0.5x TE buffer with 40 mM $MgCl_2$) is sonicated until it is fully dissolved. The stock solution of DNA origami nanoblocks (50 nM DNA origami nanoblocks in 0.5x TE buffer with 40 mM $MgCl_2$) is shaken for 5 min. Then the stock solution of DNA origami nanoblocks (17 µL, initial ratio of Ru to DNA origami nanoblocks $\sim$ 5000x) is mixed with the stock solution of the Ru-complex (283 µL). The resulting solution is shaken for several seconds until it is completely dissolved. The solution was incubated at room temperature for 30 min in the dark. After incubation time, the solution was centrifuged at 12,100 g. The supernatant was gently pipetted out to separate unbound Ru-complex from the pellet containing the Ru-complex-loaded nanoblocks. Pellets were then air dried.
The concentration of the Ru-complex was measured using the NanoDrop™ UV-Vis spectrophotometer. To measure the pellets it was necessary to dissolve them. Buffer (150 µL) was added to the pellets. The pellets were scraped and stirred with a thin plastic spatula. Then the pellets were sonicated for 5 min. If there are still a lot of undissolved pellets, the buffer was added and sonicated again for 5 min until fully dissolved.

3.6 Sample preparation for microscopy

3.6.1 Deposition on silicon substrates for AFM imaging

Si substrates were cleaned with 1 mL of pure ethanol, blow dried and plasma cleaned for 5 min. Plasma activates the Si surface to become hydrophilic.

One microliter of DNA origami solution (50 - 100 nM DNA origami nanoblocks) was dropped onto the Si wafer (0.6 cm x 0.6 cm) together with 15 µL of 10x TAE with 125 mM $MgCl_2$. Samples were incubated over an ethanol bath for an hour and were then washed with 1 mL of 50% ethanol and dried using N_2. Samples were visualized with Scanning Probe Microscope Bruker Dimension Icon in PeakForce Tapping mode with a ScanAsyst probe (40 kHz, 0.4 N/m) to detect if the prepared DNA origami corresponds to the designed 3D structure. Areas of 4 x 4 μm^2 and 2 x 2 μm^2 were scanned. Images were evaluated and flattened in Gwyddion 2.59.

3.6.2 Deposition on copper grids for TEM imaging

Negative Staining TEM

Carbon-coated copper grids were plasma treated for 45 s before use. Subsequently, 5 µL of DNA origami solution (50 - 100 nM DNA origami nanoblocks) was dropped onto the grids. The sample droplet was incubated for 30 s on the grids and then blotted away with filter paper. A 5 µL droplet of aqueous uranyl acetate was added

and immediately blotted away with filter paper. This was repeated two times. The grids were then air dried and carefully placed inside the sample holder. Samples were visualized with transmission electron microscope Jeol JEM-F200 (200 keV) for high resolution or the transmission electron microscope Jeol JEM-1400 (200 keV) for quick low resolution scans.

Cryo-TEM

A 3 - 4 µL sample of DNA origami nanoblocks with concentrations 1 - 2.8 µM were dropped onto copper grids inside a Leica EM GP2 Automatic Plunge Freezing Apparatus which was used for plunge freezing, deposition, and blotting in a controlled environment. The deposition was done at a constant temperature (20 °C) and humidity (100%) with 0 s wait time, 2 - 4 s blot time and -1 to 0 blot force. Plunging was done in a liquid ethane and the sample is transfered to a holder cooled down by liquid nitrogen to keep it frozen. Samples were visualized with transmission electron microscope Jeol JEM-F200 (200 keV).

3.7 Agarose gel electrophoresis

A 2% agarose mixture was heated until the solution was clear and 2 µL of SYBR Green I detection dye was added. The agarose solution was cooled down ($\sim$ 60 °C) and poured into a mold (using a gel comb to make wells) and further cooled down to room temperature to solidify the solution. The gel was put into the fridge for at least 30 minutes. Then, the gel was immersed in a bath of 0.5x TAE buffer with 6 mM $MgCl_2$. 10 µL of DNA origami nanoblocks or 10 µL of ruthenium-loaded DNA origami nanoblocks (initial ratio of Ru to DNA origami nanoblocks $\sim$ 800 - 900x) were mixed with 2 µL of loading dye. The resulting solutions were then loaded into the wells. Electrophoresis was performed for 35 min at 100 V, then the gels were imaged by illumination at 365 nm and 254 nm on a UV transilluminator.

3.8 Laser irradiation

Si substrates were plasma cleaned before use. Subsequently, 6 µL of DNA origami solution (1 nM DNA origami triangles) was dropped onto the Si wafer (0.5 cm x 0.5 cm). Samples were irradiated with laser EKSPLA NT-230 with OPO. Laser beams with wavelengths of 225 nm, 260 nm, 320 nm and 520 nm a pulse width of $\sim$ 4.5 - 5 ns were used. The prism was used to direct the beam perpendicular to the sample. The energy measured just above the sample was between 0.9 - 1.5 mJ/pulse over a surface area of 0.8 - 1.1 cm, which corresponded to an intensity of 2 - 5 x 10^9 W/m^2 with a fixed frequency of 20 Hz. The beam reaches its maximum output after $\sim$ 20 s, so the beam was first manually chopped and then released at its maximum output to ensure uniform intensity throughout the entire irradiation time.

To fix the irradiated samples on Si wafers, 10 µL 1x TAE buffer with 125 mM $MgCl_2$ was added and incubated for 1 h, then dried using N_2. Samples were visualized in the AFM to check sample damage. Areas of 4 x 4 μm^2 and 2 x 2 μm^2 were scanned. Images were evaluated and edited in Gwyddion 2.59.

3.9 MTT assay

The MTT assay is based on the mitochondrial reduction of MTT dye to formazan in living cells [98]. For this assay, FaDu cells were used. FaDu cells were grown in a growth medium DMEM + 10% FBS and subcultured 2 - 3 times per week. The cells were cultured in an incubator (37 °C, humidified atmosphere containing 5% CO_2). The MTT assay used in this work was patterned from the original work of L. Sala et al. [77].

3.9.1 Nanoblocks

For the 72 hrs experiment, about 4000 FaDu cells per well (100 µL) were seeded in a 96-well plate. Seeded cells were incubated overnight, then the growth medium was replaced with the medium containing different concentrations of cisplatin-loaded DNA origami nanoblocks with estimated cisplatin contents ranging from 0.1 to 100 µM or control samples containing pure DNA origami nanoblocks at concentrations matching the DNA concentrations in cisplatin-loaded DNA origami nanoblocks. The plates were then incubated for 72 hrs.

After the incubation time, MTT (2.5 mg/mL) was added to the growth medium (25 µL MTT for every 100 µL of medium). After 2 hrs of incubation, the medium was aspirated, then 150 µL of Triton X-100 in acidified (HCl) isopropyl alcohol was added to each well. The absorbance at 570 nm was measured for each well using the Infinite M200 Pro spectrophotometer. The cytotoxicity protocol is shown below.

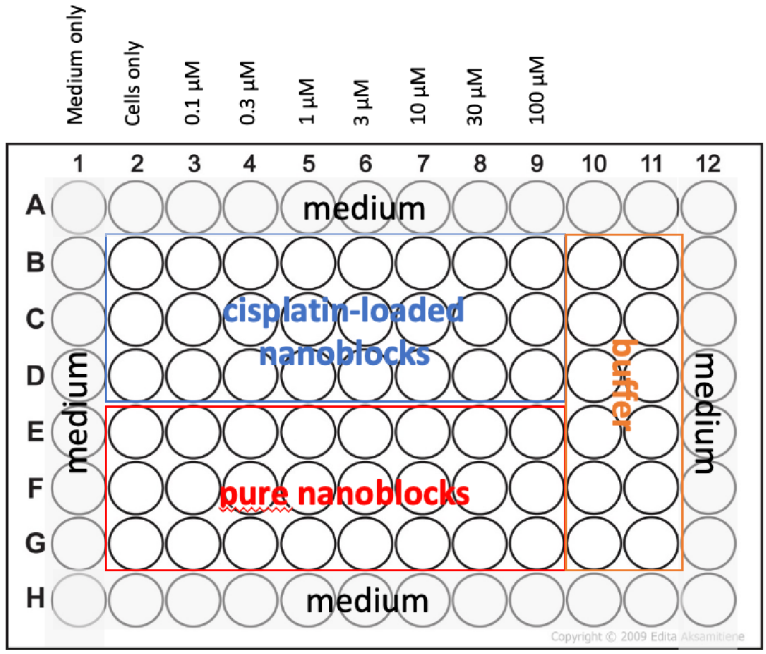

FaDu: for 72 hrs **4,000 cells**/100 µL/well, in DMEM + **10% FBS**

1×96-well plates for **one** incubation time
100 µL per well => 3-plicate x 100 µL = 300 µL minimum
pure nanoblocks (81 µL): 3761 nM
cisplatin-loaded nanoblocks (71 µL): 1158.04 µM / 3308.7 nM (DNA)

Vial	Use sterile epp. tubes!!!	Medium	Final conc. (F.C)	Volume
100	51 µL of 979 µM nano / nano-cisplatin	449 µL	100 µM	500 µL
30	105 µL vial 100	245 µL	30 µM	350 µL
10	35 µL vial 100	315 µL	10 µM	350 µL
3	35 µL vial 30	315 µL	3 µM	350 µL
1	35 µL vial 10	315 µL	1 µM	350 µL
0.3	35 µL vial 3	315 µL	0.3 µM	350 µL
0.1	35 µL vial 1	315 µL	0.1 µM	350 µL

1158.04 µM dilute with 10% buffer to 979 µM, corresponding to 1st row of the table
38 µL pure nanoblocks + 462 µL medium ≅ 285 nM DNA origami, corresponding to 1st row of the table

Figure 3.1: Cytotoxicity protocol: DNA origami nanoblocks modified by cisplatin (with pure DNA origami nanoblocks and pure buffer as controls).

3.10 SRB Assay

SRB assay is based on the binding of SRB dye to proteins in cells [98]. FaDu cells were also used in this assay. FaDu cells were grown in a growth medium DMEM + 10% FBS and subcultured 2 - 3 times per week. The cells were cultured in an incubator (37 °C, humidified atmosphere containing 5% CO_2).

3.10.1 Nanoblocks

For the 48 hrs incubation, about 5000 FaDu cells per well (100 µL) were seeded in a 96-well plate. For the 72 hrs experiments, about 3000 FaDu cells per well (100 µL) were seeded in a 96-well plate. For the 96 hrs, about 3000 FaDu cells per well (100 µL) were seeded in a 96-well plate. Seeded cells were incubated overnight, then the growth medium was replaced with the medium containing different concentrations of Ru-complex-loaded DNA origami nanoblocks with estimated Ru contents ranging from 0.1 to 30 µM or control samples containing pure DNA origami nanoblocks at concentrations matching the DNA concentrations in Ru-complex-loaded DNA origami nanoblocks. The plates were then incubated for the desired incubation times.

After incubation, the medium was aspirated. The cells were fixed by adding 10% cold TCA (100 µL) and incubated for 1 h at 4 °C in the dark. After 1 h, the cells were washed twice with distilled H_2O (200 µL). Cells were stained with 100 µL 0.1% SRB dissolved in 1% acetic acid for at least 15 minutes. After staining, the cells were washed twice with 1% acetic acid (200 µL) and air dried. The staining was solubilized with 10 mM un-buffered tris base (100 µL) and then transfered 100 µL of the dye was transfered into each well. The absorbance at 540 nm was measured for each well using Infinite M200 Pro spectrophotometer. The cytotoxicity protocol is shown below.

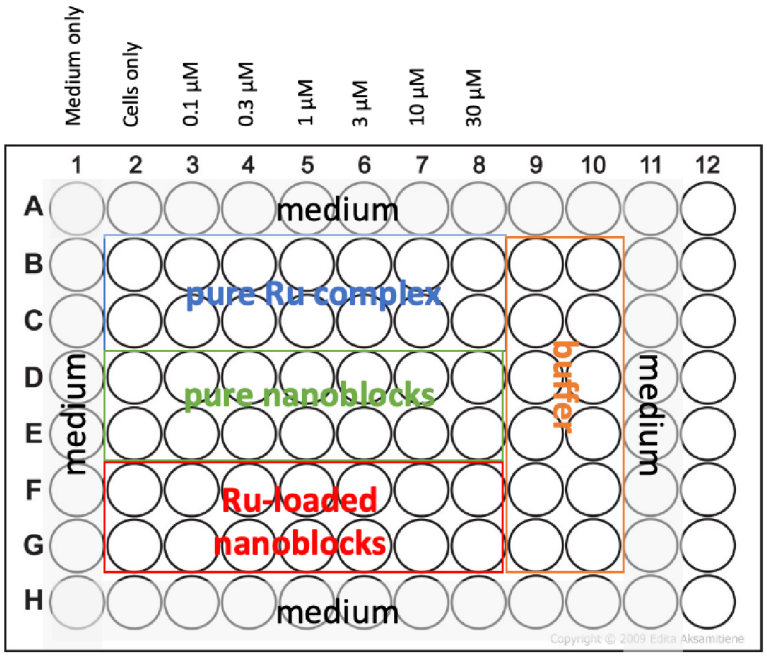

FaDu: for 96 hrs **3,000 cells**/100 µL/well, in DMEM + **10% FBS**
FaDu: for 72 hrs **3,000 cells**/100 µL/well, in DMEM + **10% FBS**
FaDu: for 48 hrs **5,000 cells**/100 µL/well, in DMEM + **10% FBS**

1×96-well plates for **one** cell line and **one** incubation time (multiply by 2 for 48+72+96 hrs incubations)
100 µL per well => 2-plicate x 100 µL = 200 µL minimum
Ru complex: 372 µM
pure nanoblocks: 900 nM
Ru-loaded nanoblocks: 327 µM / 50 nM (DNA)

Vial	Use sterile epp. tubes!!!	Medium	Final conc. (F.C)	Volume
30	70 µL of 300 µM Ru	630 µL	30 µM	370 µL
	70 µL of 300 µM nano-Ru	630 µL	30 µM	
	70 µL of 45 µM nano	630 µL	4.5 µM	
10	160 µL vial 30	320 µL	10 µM	480 µL
3	50 µL vial 30	450 µL	3 µM	500 µL
1	50 µL vial 10	450 µL	1 µM	500 µL
0.3	50 µL vial 3	450 µL	0.3 µM	500 µL
0.1	50 µL vial 1	450 µL	0.1 µM	500 µL

327 µM Ru-loaded nanoblocks dilute with 10% buffer to 300 µM, corresponding to 1st row of the table

Figure 3.2: Cytotoxicity protocol: DNA origami nanoblocks modified by ruthenium complex (with pure nanoblocks and pure Ru-complex as controls).

4 Results and discussion

The main goal of the thesis was to explore the potential of DNA origami nanostructures for applications in medicine. Thus, I tried 2 types of drugs with different binding mechanisms to DNA - an Ru-complex and cisplatin. The Ru-complex intercalates into DNA whereas cisplatin covalently binds to DNA. I then tried to optimise the drug loading of these drugs into DNA origami nanostructures and determined their cytotoxicity in FaDu cells as a tumour cell model. Participating on a more complex study towards applications of DNA origami nanostructures in sensing applications, I also explored the stability of DNA origami in solution under laser irradiation (with 2D DNA nanotriangles as an example) and tried functionalizing a potential sensing molecule like G-quadruplex on 2D DNA origami nanoframes.

For the first part of my work, I prepared 3D DNA origami in the shape of a nanoblock according to Zhong's method as the choice nanostructure for drug loading experiments [79]. The preparation of DNA origami and its deposition is not trivial, various defects may occur; therefore, some optimization of the protocol is needed. The preparation of DNA origami nanoblocks and its optimization for loading with cisplatin is discussed in Section 4.1. In Section 4.2, the results of the cytotoxicity of cisplatin-loaded nanoblocks are shown. Similarly, results of the loading of the Ru-complex on the nanoblocks are explained in Section 4.3 and the corresponding cytotoxicity is evaluated in Section 4.4. The effect on tumour cells of both drugs (free and loaded on the nanoblocks) are then compared in Section 4.5.

The second part involves testing the stability of DNA origami under light and the incorporation of a sensing molecule. For the stability studies under laser irradiation, the preliminary results of irradiated DNA origami nanostructures are shown in Section 4.6. The preparation of DNA origami nanoframes with a G-quadruplex system is shown in section 4.7. The results in the second part of my work can provide some insight on stability and functionalization of DNA origami nanostructures for possible applications in sensors that can also be used in medicine.

4.1 Cisplatin-loaded DNA origami

At first, I examined the effect of the concentration of Mg^{2+} cations in the buffer. DNA origami nanoblocks were synthesized in the prescribed magnesium-rich folding buffer. The formation of the DNA origami nanoblocks was confirmed by Cryo-TEM as shown in Fig. 4.1. The dimensions of the particles correspond to the expected dimensions of the 6 x 6 x 64 nt nanoblocks as designed.

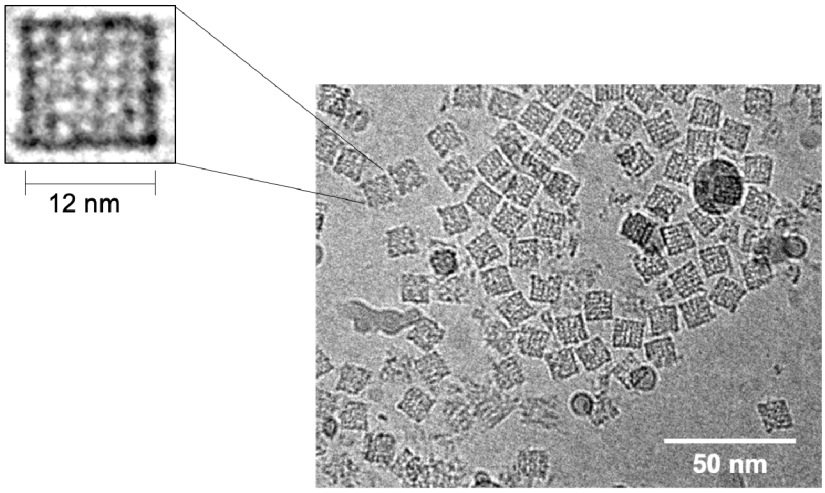

Figure 4.1: CryoTEM image of pure DNA origami nanoblocks in their native state, 100kx mag. [**author**].

For cisplatin loading, it is important to reduce tris and Cl^- anions in the loading buffer as much as possible [77]. If the loading buffer contains more Cl^- anions, a reverse reaction would occur during the aquation process (described in subsection 2.2.1, Fig. 2.7) and more cisplatin would be formed than the required Pt^{2+} with water molecules bonded to it. During the aquation process, tris is also able to chelate Pt^{2+} cation instead of H_2O molecules and a competition between tris and H_2O occurs. Therefore, there is an effort to prepare a loading buffer with a low content of tris and Cl^- anions, although a certain quantity of Mg^{2+} cations is still needed for the stability of the DNA origami nanostructures.

Sample AFM and TEM images, demonstrating the effect of the loading process using different buffer solutions on the DONs are in Fig. 4.2 In both images, it can be noticed that the low concentration of Mg^{2+} cations in the buffer causes unwanted aggregation and deformation of DNA origami nanoblocks. I found out that the concentration of $MgCl_2$ 0.1 mM is low enough to load cisplatin, but still sufficient to have mostly intact DNA origami nanoblocks. If the concentration of Mg^{2+} cations is reduced, the DNA origami nanoblocks are damaged. If the concentration of $MgCl_2$ is increased, less cisplatin will load to the DNA origami nanoblocks. This can already be observed in the AFM but it does not have enough

resolution to observe structural changes in the 3D nanostructures, so TEM was used instead. Although the deformation could be mostly due to the depletion of Mg^{2+} cations, it is also to be noted that further deformations can occur in TEM imaging from sample preparation/staining to radiation damage during imaging.

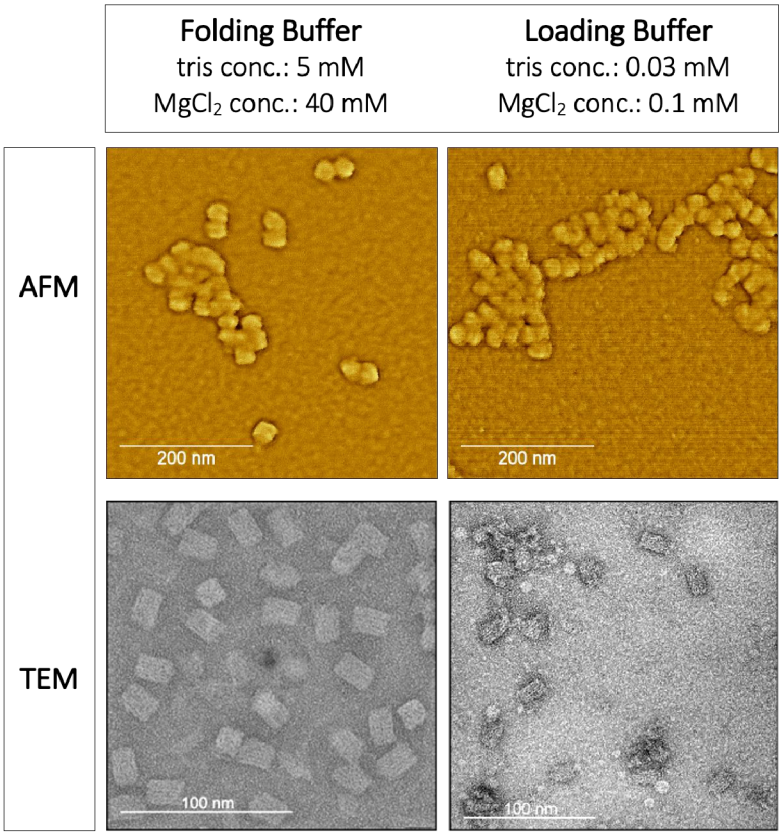

Figure 4.2: Deposition of DNA origami nanoblocks using different concentrations of Mg^{2+} cations. AFM images showing deposition on Si substrate with folding buffer containing 40 mM Mg^{2+} cations (top left) and with loading buffer containing 0.1 mM Mg^{2+} cations (top right). TEM images showing deposition on carbon substrate with folding buffer containing 40 mM Mg^{2+} cations (bottom left, 100kx mag.) and with loading buffer containing 0.1 mM Mg^{2+} cations (bottom right, 50kx mag.) [**author**].

After buffer exchange, ICP-MS analysis was performed to find out how many Pt atoms and cisplatin have bound to the DNA origami nanoblocks. Solutions with different concentrations of cisplatin were mixed with DNA origami nanoblocks, incubated for some time, and then filtered through 100 kDa MWCO Amicon filters to get rid of unbound cisplatin. Filtered samples were analysed by ICP-MS. Fig. 4.3A shows the effect of changing the cisplatin concentration in the stock solution. As the concentration of cisplatin in the stock solution increases, the amount of loaded cisplatin increases after 8 hrs. Fig. 4.3B shows the effect of

different loading times. After investigating the effects of loading time and initial cisplatin concentration, I found out that the maximum cisplatin loading possible that will still have intact nanostructures occurs at around 16 hrs with an initial ratio of cisplatin to DNA origami of 2400:1. This results in $\sim$ 350 bound Pt per nanostructure. Although in principle, more Pt can still be loaded onto the nanoblocks because a plateau has not been reached yet, after reaching $\sim$ 350 bound cisplatin/DNA origami nanoblock, the DNA origami nanostructures start to deform. Thus, I used this as the upper limit for the loading conditions used for the cytotoxicity experiments.

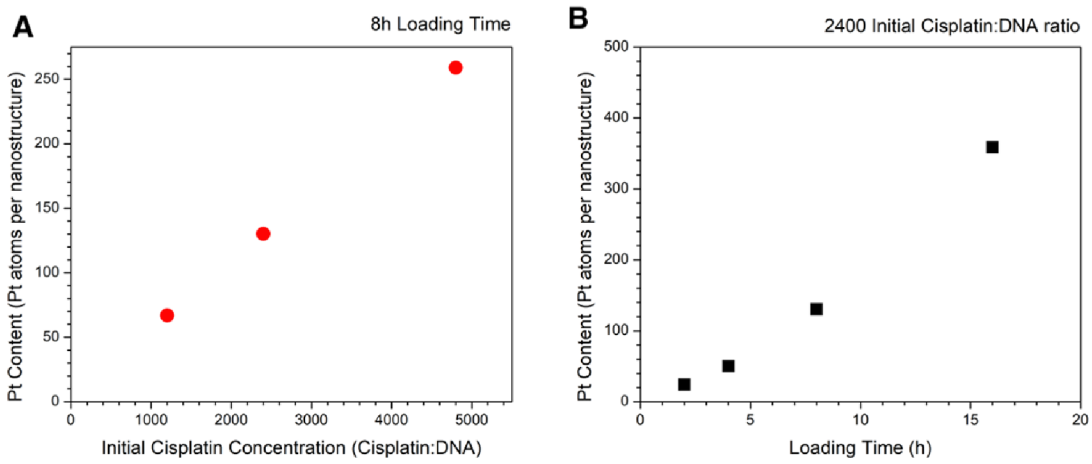

Figure 4.3: ICP-MS results of cisplatin-loaded DNA origami nanoblocks. a) Effect of cisplatin concentration during loading, and b) Effect of loading time [**author**].

Fig. 4.4 shows the TEM image of the nanoblocks at our chosen loading conditions. Apparently, because cisplatin can form intrastrand and interstrand cross-links, it can enhance agglomeration, as shown in the red circle. However, there are still a lot of intact, isolated DNA origami nanoblocks, as shown in the green circles.

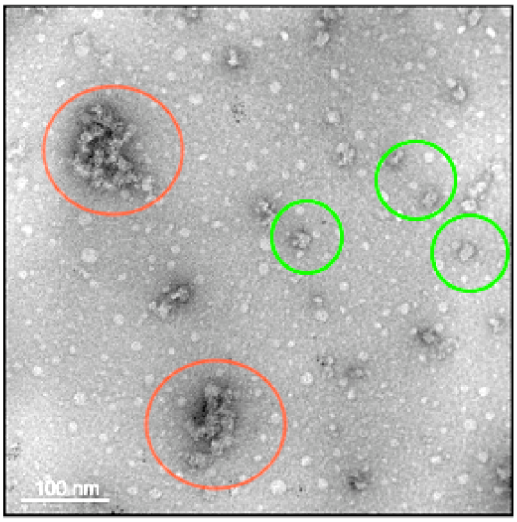

Figure 4.4: TEM image of cisplatin-loaded DNA origami nanoblocks, 30kx mag. [**author**].

4.2 Cytotoxicity of cisplatin-loaded DNA origami

To evaluate the cytoxicity of pure DNA origami nanoblocks and cisplatin-loaded DNA origami nanoblocks, I have done the MTT assay on FaDu cells that were incubated for 72 hrs with pure and cisplatin-loaded DNA origami nanoblocks. FaDu cells were visualized by optical microscope to check their condition before use (Fig. 4.5).

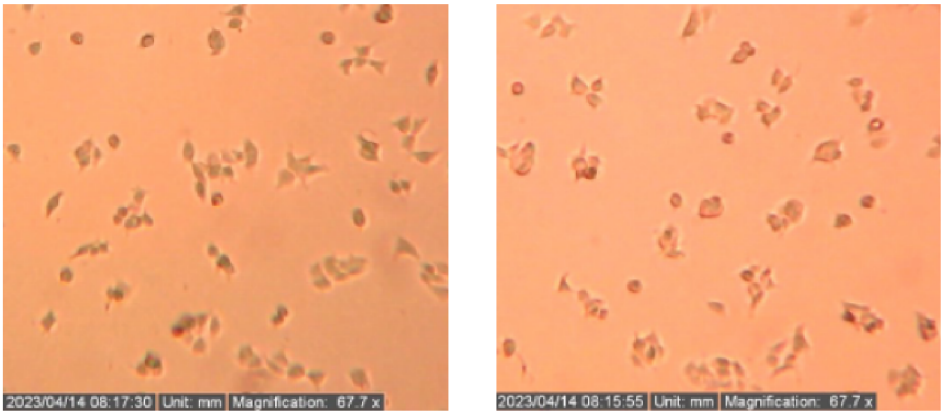

Figure 4.5: FaDu cells in the cell culture (left) and after changing the growth medium for cytotoxicity experiments (right), 67.7x mag. [**author**].

The graph in Fig. 4.6 shows the dependence of the cell viability on the concentration of cisplatin and the corresponding DNA concentration for the nanoblocks. It has been already shown in the publications of Zhong and Sala [77][79] that pure DNA origami are not toxic, which was also confirmed in the present experiment (blue squares in Fig. 4.6). Cisplatin-loaded DNA origami nanoblocks (orange circles in Fig. 4.6) become more toxic with increasing cisplatin concentrations. The IC_{50} values, or the concentration at which 50% of cell viability is achieved, can be estimated from the cell viability curves. The values are shown in the table above Fig. 4.6. The IC_{50} for pure cisplatin and cisplatin-loaded triangles from the work of Sala et al. are included for comparison [77].

Based on these IC_{50} values, it appears that to achieve the cytotoxicity of pure cisplatin, a higher concentration of cisplatin in DNA origami nanoblocks is needed. This does not necessarily mean that the cisplatin-loaded nanoblocks are inferior. For drug delivery applications, DNA origami nanoblocks have the ability to concentrate cisplatin in them to deliver only nM concentration of the drug carrier. Furthermore, it introduces the possibility of targeted delivery thereby, reducing side effects on healthy cells.

The IC_{50} values also show that cisplatin-loaded DNA origami nanoblocks are less toxic than cisplatin-loaded triangles, based on the Pt concentration equivalent. This is probably due to agglomeration problems discussed in the previous section that may affect the uptake. It is important to mention that cytotoxicity is studied on cancer cells. To use these DNA origami nanoblocks for drug delivery applications, it is appropriate to investigate the targeting of these nanoblocks to cancer cells to diminish the effects on surrounding healthy cells. For the future, tracking uptake and drug release *in vivo* was proposed, which is currently being initiated by a group at the Center for Advanced Preclinical Imaging (CAPI) at the First Faculty of Medicine at Charles University in Prague.

Incubation Time 72 h	IC-50	
	cisplatin conc. [µM]	DNA conc. [nM]
cisplatin	2.1 ± 0.2	–
cisplatin-loaded triangles	20 ± 3	22 ± 3
cisplatin-loaded nanoblocks	33 ± 12	94 ± 33
pure nanoblocks	–	>> 285 nM

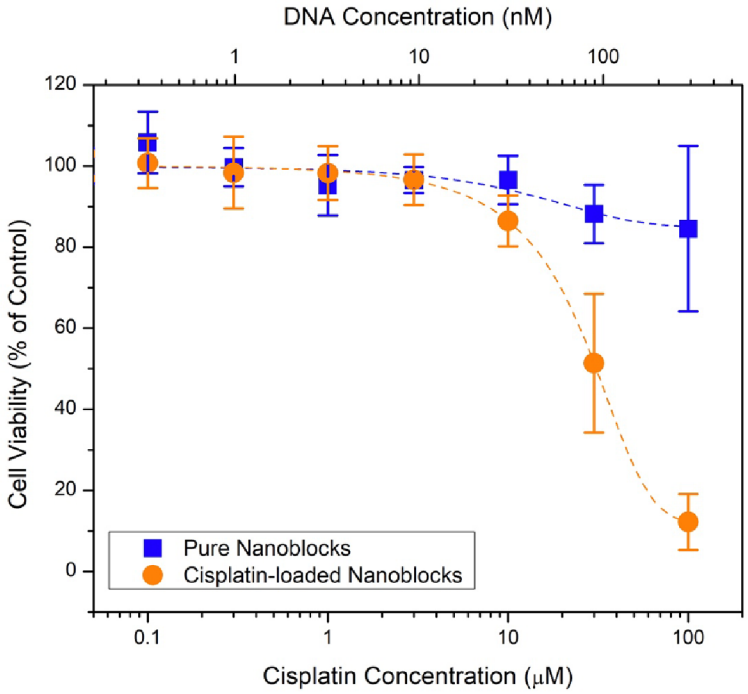

Figure 4.6: Cell viability curves of pure and cisplatin-loaded DNA origami nanoblocks. The cell viability of treated cells is shown as a percentage of untreated cells (control). The results plotted in the graph are calculated as the mean ± SD values of 3 independent experiments done in triplicates. The IC_{50} table is supplemented with values for pure cisplatin and cisplatin-loaded DNA origami nanotriangles also on FaDu cells from the work of Sala et al. [**author**][77].

4.3 Ruthenium complex-loaded DNA origami

I also used a Ru-complex to explore another type of DNA-binding mechanism in comparison to cisplatin. This model Ru-complex intercalates into DNA and is optically active, so it is also easier to track concentrations with the UV-Vis spectrophotometer compared to cisplatin. Also, the ruthenium complex can be loaded to DNA origami nanoblocks in the folding buffer without damaging the structure.

UV-Vis analysis was performed to find out how many Ru-complexes have bound to the DNA origami nanoblocks. For the analysis it was necessary to create a calibration curve for different concentrations of Ru-complex in the DNA origami nanoblocks. UV-Vis spectra were obtained for different concentrations of Ru-complex mixed with the same concentration of DNA origami nanoblocks (Fig. 4.8). The absorbance at 372 nm and 439 nm was measured using NanoDrop™ One Microvolume UV-Vis spectrophotometer. The absorbance is measured in this wavelength range because DNA origami nanoblocks are not absorbing at these wavelengths, therefore, the signals are only from Ru-complex. The high peak at 282 nm corresponds to the signals of the Ru-complex, free ligand, and DNA origami nanoblocks so it was not utilized.

Although the loading in this case can be done in the folding buffer. Thereby not disturbing so much of the structure, the main problem with this system comes from the limited solubility of the Ru-complex in the aqueous solution. Ru-complex-loaded DNA origami nanoblocks aggregate immediately and we also lose some of the sample during preparation. The loss of sample is caused by either incomplete dispersion of pellets or pellets sticking to container walls. However, even with some losses, I was able to load the Ru-complex into the nanoblocks. Fig. 4.7 shows that 16.5 ± 1.9 % of Ru was bound to the DNA origami nanoblocks (the ratio of Ru to DNA origami nanoblocks is 825 ± 96) which is much higher than the highest value reached for cisplatin. This is probably the main cause of the increased agglomeration.

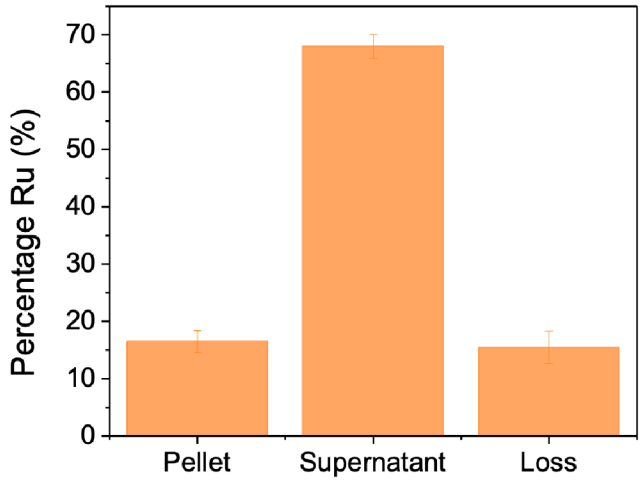

Figure 4.7: Loading of Ru-complex to DNA origami nanoblocks: pellets (Ru-complex-loaded DNA origami nanoblocks), supernatant (unbound Ru-complex) and the estimated sample loss [**author**].

Calibration Curve		
Ru complex conc. [μM]	DNA conc. [nM]	Ru:DNA Ratio
0	46	0
1	46	22
3	46	65
10	46	224
30	46	654
90	46	1957

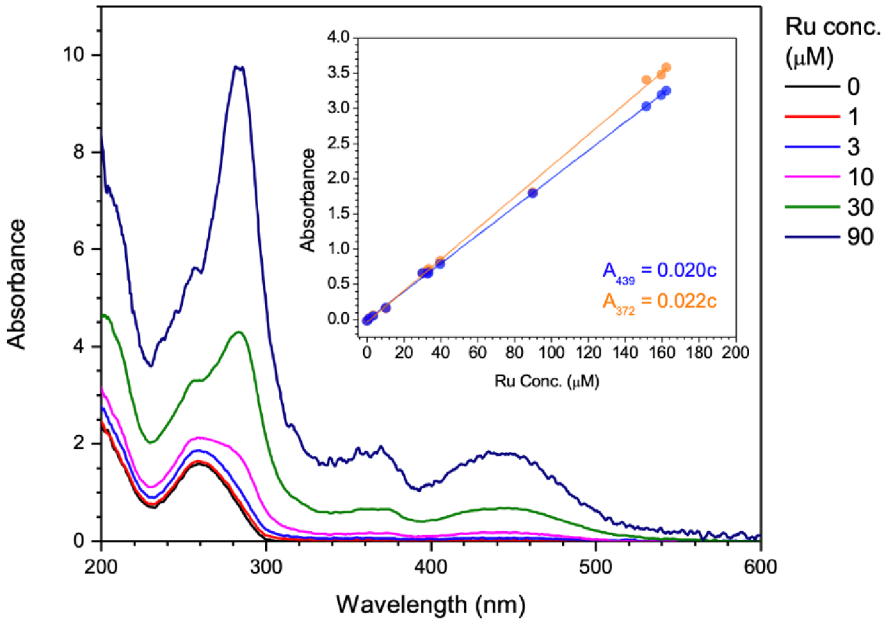

Figure 4.8: UV-Vis spectrum of Ru-complex-loaded DNA origami nanoblocks with the corresponding calibration curve for different concentrations of Ru-complex in the DNA origami nanoblocks. The concentrations of DNA nanoblocks and Ru-complex used to construct the curve are listed in the table above [**author**].

As with cisplatin, I examined the structure of pure nanoblocks and Ru-complex-loaded DNA origami nanoblocks using AFM. The result is shown in Fig. 4.9. Although the resolution is not sufficient, the dimensions and appearance of the AFM images are consistent with the TEM-confirmed structures in Fig. 4.1, which means that the assembly of the nanoblocks for Ru-complex loading was successful. In Fig. 4.10, AFM images of nanoblocks loaded with the Ru-complex demonstrate that the structure is more or less preserved after the loading procedure.

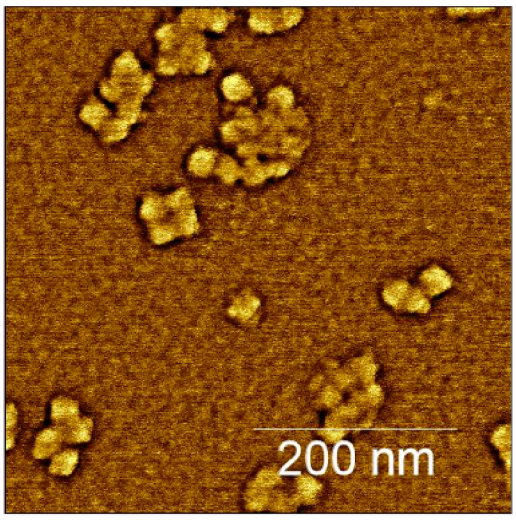

Figure 4.9: AFM images of pure DNA origami nanoblocks, deposited on a Si substrate [**author**].

As discussed earlier, the main disadvantage of using the Ru-complex is its limited solubility in H_2O. This property is also evident in Ru-complex-loaded DNA origami nanoblocks. In trying to overcome this, I tried to gently sonicate the Ru-complex-loaded DNA origami nanoblocks. Fig. 4.10 shows the difference between dissolved pellets and sonicated pellets. As shown, simply dissolving the Ru-complex-loaded DNA origami nanoblocks is not enough, it needs to be sonicated to avoid aggregates forming.

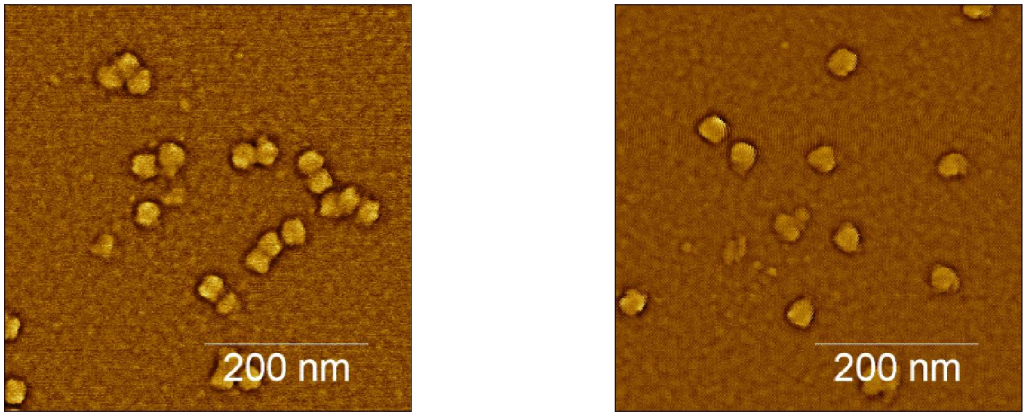

Figure 4.10: AFM images, of Ru-complex-loaded DNA nanoblocks deposited on an Si substrate before sonication (left) and after 5 min of sonication (right) [**author**].

In addition to AFM, agarose gel electrophoresis (AGE) was performed to examine the stability of Ru-complex-loaded DNA origami nanoblocks. Fig. 4.11 compares the stability of pure nanoblocks and Ru-complex-loaded DNA origami nanoblocks. All lanes have approximately the same concentration of DNA. SYBR Green I dye binds to DNA in the same way as Ru-complex, so the bands may disappear or fade, as well as we can see some agglomeration.

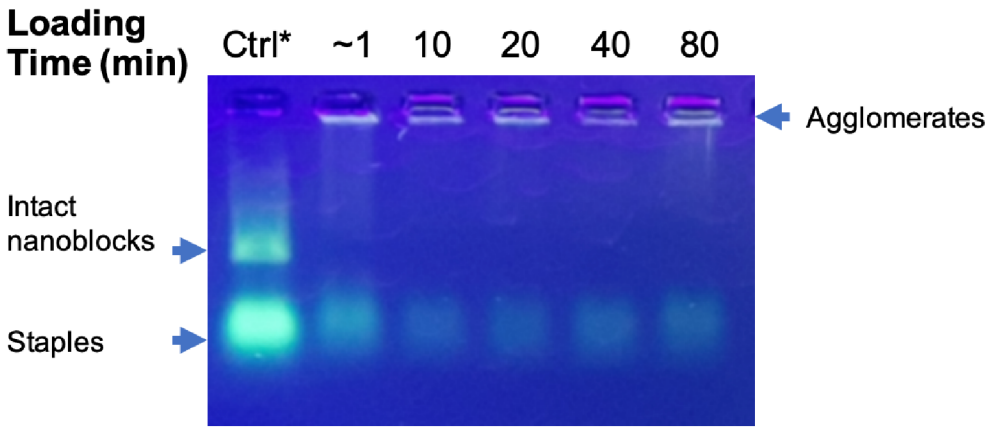

Figure 4.11: AGE for pure DNA origami nanoblocks (control) and Ru-complex-loaded DNA origami nanoblocks. [**author**].

Ru-complex is easier to track than cisplatin due to its sensitivity to light. Fig. 4.12 shows that Ru-complex fluoresces only after binding to DNA.

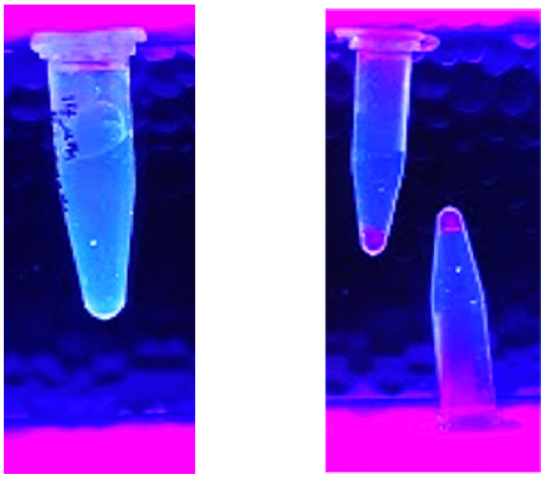

Figure 4.12: Illuminated sample of pure Ru-complex (left) and Ru-complex-loaded DNA origami nanoblocks (right) [**author**].

4.4 Cytotoxicity of ruthenium complex-loaded DNA origami

To detect the toxicity of pure Ru-complex, pure DNA origami nanoblocks and Ru-complex-loaded DNA origami nanoblocks, I have done the SRB assay on FaDu cells that were incubated for 48 hrs, 72 hrs and 96 hrs with the Ru-complex, pure DNA origami nanoblocks and Ru-complex-loaded DNA origami nanoblocks. According to the study by Cervinka et al., Ru-complexes affect mitochondrial metabolism which will interfere with the MTT analysis as the reagent acts on the mitochondria [98]. Therefore, instead of the MTT assay that I used for cisplatin, the SRB assay was applied for the Ru-complex (Fig. 4.13). The amount of dye corresponds to the number of cells left after treatment. Images of FaDu cells were visualized by an optical microscope. Fig. 4.14 shows FaDu cells with Ru-complex-loaded DNA origami nanoblocks, these Ru-complex-loaded nanostructures may also aggregate, as shown in the red circle.

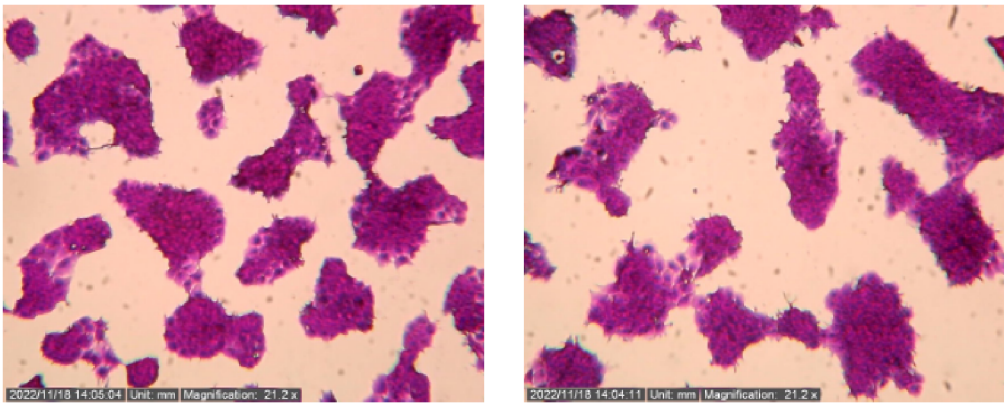

Figure 4.13: FaDu cells incubated for 48 hrs (left) and 72 hrs incubated FaDu cells (right) fixed and stained with SRB dye, 21.2x mag. [**author**].

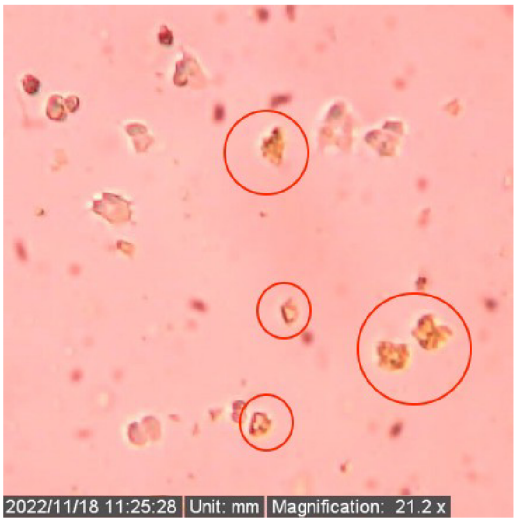

Figure 4.14: FaDu cells with aggregated Ru-complex-loaded DNA origami nanoblocks, 21.2x mag. [**author**].

Graphs 4.15, 4.16 and 4.17, show the dependence of the cell viability on the concentration of the Ru-complex in the pure DNA origami and Ru-complex-loaded DNA origami nanostructures. The pure Ru-complex (red) shows no pronounced toxicity up to 10 µM for all incubation times. At 30 µM of Ru-complex concentration, a slight decrease in cell viability of FaDu cells is observed for all time points. This is summarized in Fig. 4.18 where the cell viabilities of FaDu cells incubated with pure Ru-complex and Ru-complex-loaded nanoblocks are compared to the cell viability of the pure DNA origami nanoblocks. Between 48 hrs and 72 hrs, the cell viability decreases significantly and then stabilizes up to 96 hrs. Unfortunately, this is the highest concentration in the cell media that we can achieve for this Ru-complex due to solubility issues as evidenced by the image of the aggregates in Fig. 4.14. Ru-complex-loaded DNA origami nanoblocks (blue) exhibit the same behavior as the pure Ru-complex showing that the observed toxicity of the Ru-complex is preserved even when loaded into the DNA origami nanoblocks.

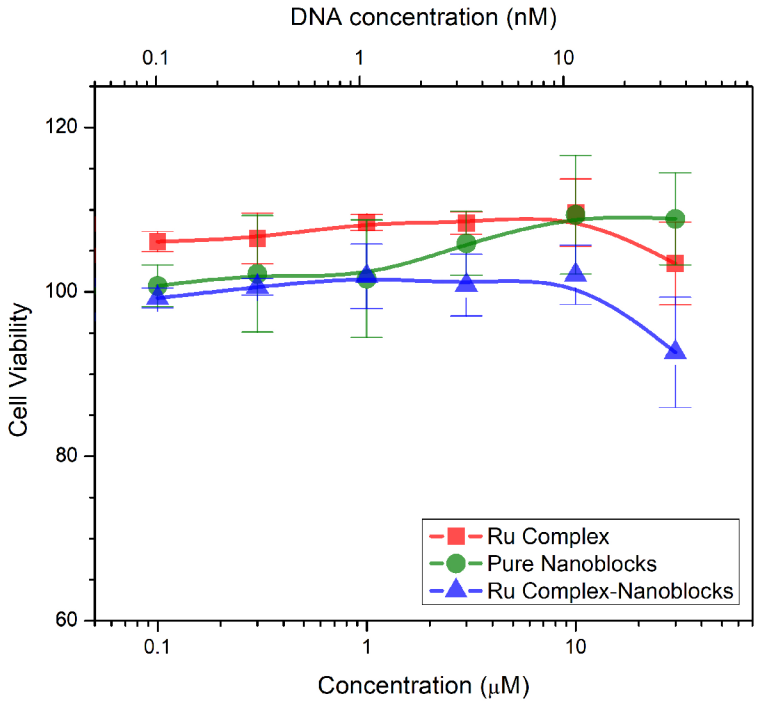

Figure 4.15: Cell viability curves for pure Ru-complex, pure and Ru-complex-loaded DNA origami nanoblocks after 48 hrs incubation time. The cell viability of treated cells is shown as a percentage of untreated cells (control). The results plotted in the graph are calculated as the mean ± SD values of 3 independent experiments done in duplicates [**author**].

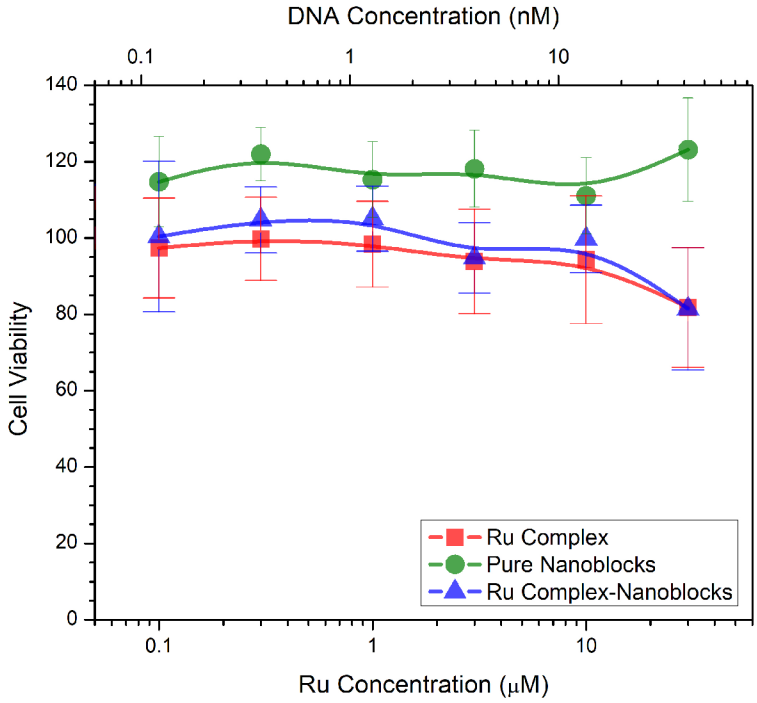

Figure 4.16: Cell viability curves for pure Ru-complex, pure and Ru-complex-loaded DNA origami nanoblocks after 72 hrs incubation time. The cell viability of treated cells is shown as a percentage of untreated cells (control). The results plotted in the graph are calculated as the mean ± SD values of 3 independent experiments done in duplicates [**author**].

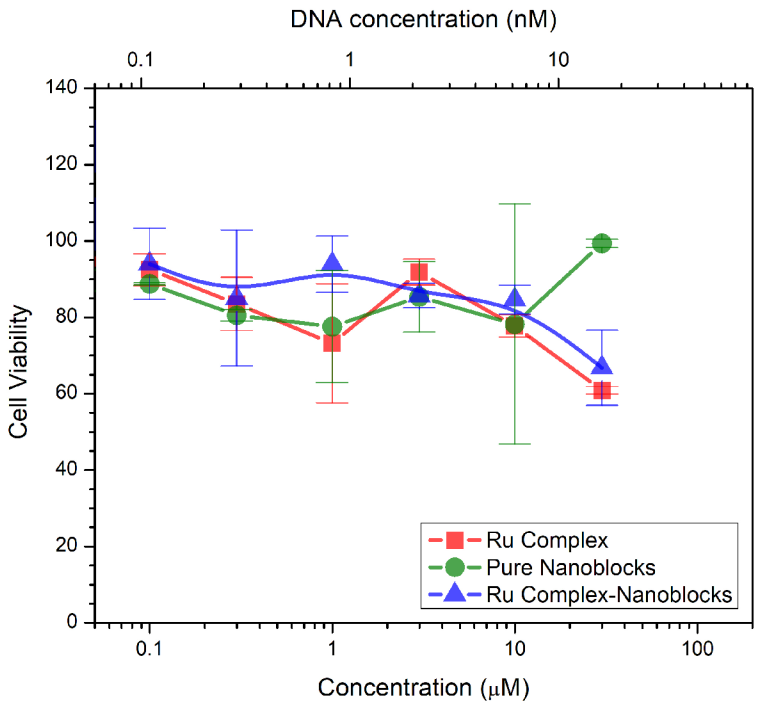

Figure 4.17: Cell viability curves for pure Ru-complex, pure and Ru-complex-loaded DNA origami nanoblocks after 96 hrs incubation time. The cell viability of treated cells is shown as a percentage of untreated cells (control). The results plotted in the graph are calculated as the mean ± SD values of 3 independent experiments done in duplicates [**author**].

4.5 Comparison between cisplatin and ruthenium complex

Since it is not possible to calculate IC_{50} values for the Ru-complex, the only possibility is to compare the cell viabilities at the highest concentration (30 µM) of Ru-complex used against of cisplatin-loaded and pure DNA origami nanoblocks.

The values in table (Fig. 4.18) show that the pure Ru-complex is less cytotoxic drug than pure cisplatin in tumour cells. This is consistent when comparing the IC_{50} values of cisplatin and the Ru-complex in certain cell lines in literature [65]. This is probably due to less binding of the Ru-complex to the DNA in the cells because intercalation is weaker than covalent bonds. The table also shows that Ru-complex-loaded DNA origami nanoblocks are less toxic than cisplatin-loaded DNA origami nanoblocks. Aside from the differences in cytotoxicity of loaded drugs, there is also some problem with agglomeration for the less soluble Ru-complex-loaded DNA nanoblocks which could have contributed to their lower cytotoxicity.

To use these DNA origami nanoblocks for drug delivery applications, it is appropriate to optimize them for targeting so that the cytotoxicity can be concentrated into the tumour cells and spare the healthy cells around, reducing possible side effects. This is possible because of the functionalizable nature of DNA origami nanostructures. For the future, as I mentioned earlier, it is proposed to track the uptake and release *in vivo*. Moreover, due to issues with solubility it would be best to explore also other water-soluble and DNA intercalating Ru-complexes.

Comparison of Cell Viability at highest concentration (30 µM)	
Incubation Time 72 h	Cell Viability [% of Control]
cisplatin	~ 25
cisplatin-loaded nanoblocks	~ 50
ruthenium complex	~ 80
ruthenium-loaded nanoblocks	~ 80

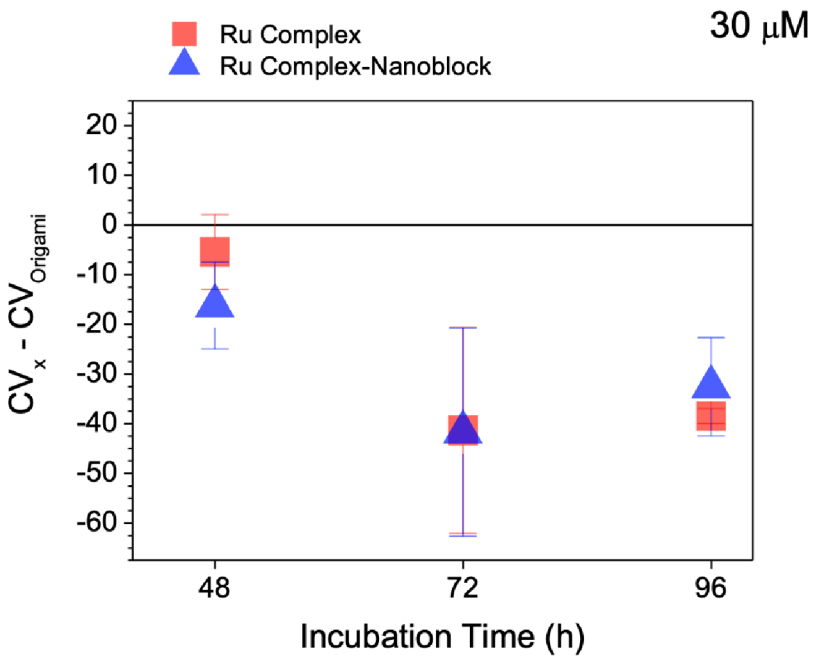

Figure 4.18: Observed cell viabilities at ∼ 30 µM concentration of pure Ru-complex, and cisplatin- and Ru-loaded nanoblocks from this work. Values for pure cisplatin is included from the work of Sala et al., for comparison. Comparison of cell viability at 30 µM drug concentration of the pure Ru-complex and the Ru-complex-loaded nanoblocks [**author**][77].

4.6 Laser irradiation of 2D DNA origami

For desired applications of DNA origami in sensing, it is crucial to evaluate DNA origami stability upon illumination with high brightness light sources such as lasers commonly used in sensing, e.g. identification of specific markers in blood using light in the UV-VIS region. I investigated DNA origami damage by light in the wavelength range from 225 nm to 520 nm, which can give some insight later for DNA origami-based sensor designs. Studying the stability of DNA origami is an essential part, and will be described in an upcoming publication which I co-authored with people from J. Heyrovský Institute of the CAS. I used 2D DNA origami triangles as a representation of 2D DNA origami designs as they are frequently used in literature for sensing applications [99][100] and are already available in the research group.

I prepared 2D triangular DNA origami and irradiated them with laser light of various wavelengths with doses up to 16 mJ/mm^2. AFM imaging was performed to evaluate the stability of DNA origami triangles. Fig. 4.19 shows how DNA origami is damaged at high doses of laser irradiation at different wavelengths. We can see that the damage copies the UV-VIS absorption spectrum of DNA, which is presented in Fig. 4.20 and therefore, the damage can be clearly assigned to electronic excitation of DNA within the origami nanostructure. At 520 and 320 nm, we cannot see any damage even at the highest doses of radiation. At 225 nm some of the triangles are still present but most of them are decomposed into fragments having structure of origami tiles. At 260 nm, where the DNA absorption peaks, the structures are completely decomposed. We can conclude that the probing wavelengths in sensing applications with DNA origami nanostructures should avoid the DNA excitation wavelengths.

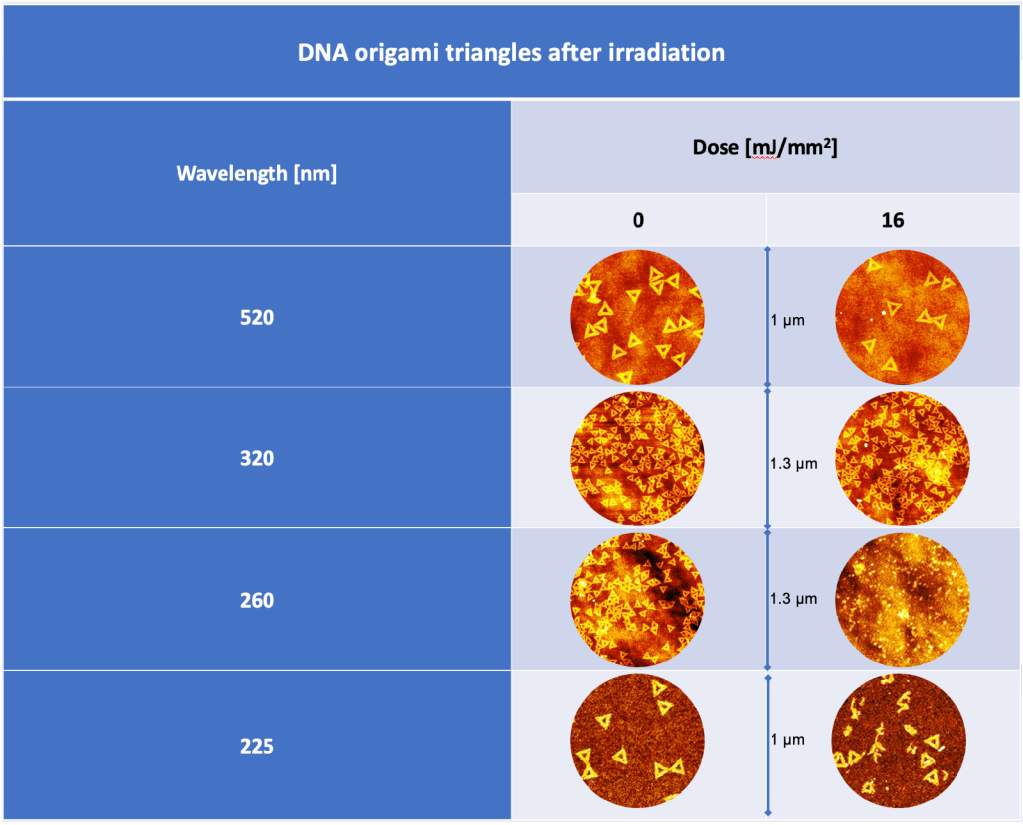

Figure 4.19: AFM image of DNA origami triangles irradiated with lasers at various wavelengths [**author**].

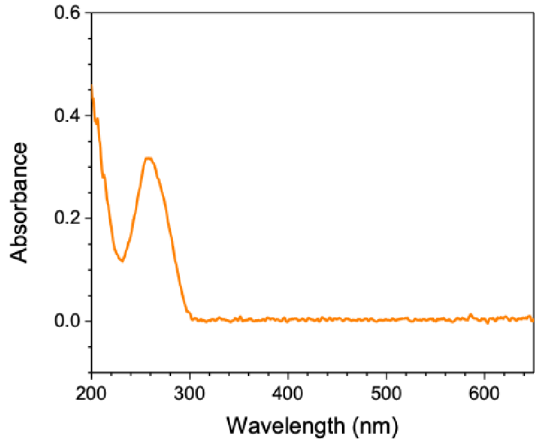

Figure 4.20: UV-Vis spectrum of DNA origami [**author**].

4.7 Functionalizing DNA origami nanostructures with a sensing molecule

As described in the theoretical part, one of the interesting sensing molecules with high selectivity to specific ions and biomolecules are G-quadruplexes. In the present work, I therefore performed some pilot studies towards their utilization for sensing applications in our group.

The goal was to incorporate G-quadruplexes and check if they are formed in DNA origami nanostructures. I used the nanoframes since they are already available in the research group and it can incorporate enough long dsDNA to study secondary DNA structure effects [92]. The frame contained 2 positions for DNA strands of interest (Fig. 4.21). I used oligomers that contain a GQ-forming sequence in the center of the top position in the frame. The bottom position is reserved as control sequence. I prepared 2D DNA origami nanoframes using the protocol by Endo et al. [92]. Fig. 4.22 shows empty DNA origami nanoframes I synthesized to test the protocol.

Figure 4.21: Scheme of frame with incorporate G-quadruplex [**author**].

With an unfolded GQ (which happens without K^+), since the G-quadruplex-forming sequence is long, I expect that the parallel DNA strands in the middle of the frame will not be well-defined. The AFM image in Fig. 4.23 (left) shows how the long unfolded strand looks like in the frames when there is no significant amount of K^+ present. When K^+ is added into the buffer, the formation of GQ is favored and we see tighter parallel strands in the middle of the frame Fig. 4.23 (right). This is also consistent with what has been observed by Endo et al. [92].

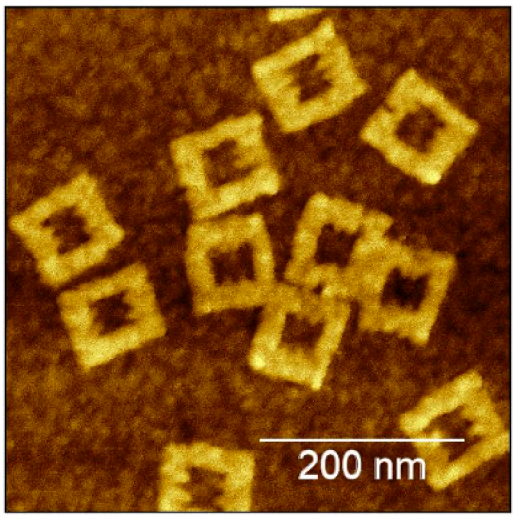

Figure 4.22: AFM image of empty DNA origami frames on Si substrate [**author**].

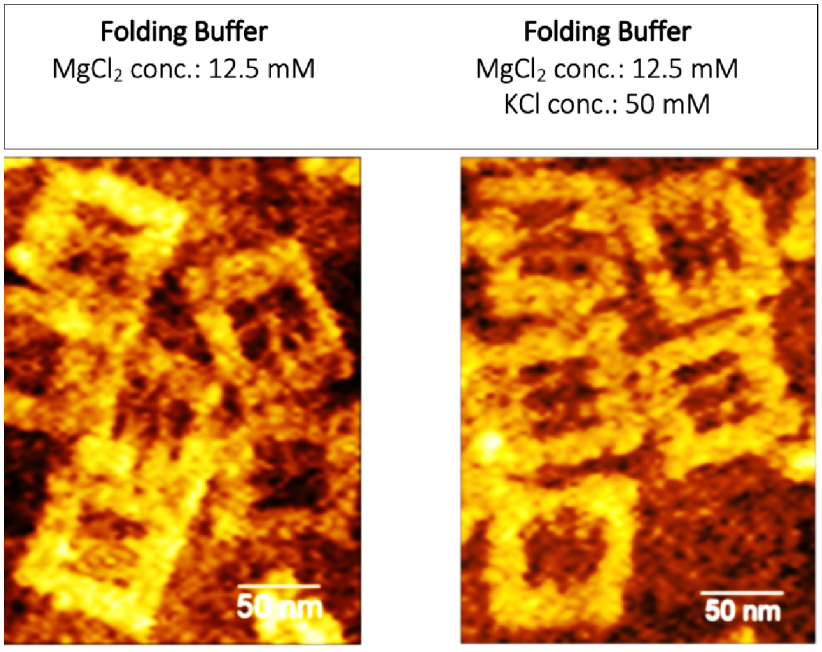

Figure 4.23: AFM images of DNA origami frames with incorporated GQs, deposition on Si substrate with folding buffer containing 12.5 mM Mg^{2+} cations (left) and with folding buffer containing 50 mM K^{+} cations (right) [**author**].

In the future, the research group plans to optimize this system for sensing applications building on the preliminary results of this work. This can be done by tagging the DNA origami with fluorescent molecules and/or nanoparticles that can be sensitive to the binding conditions or formation of G-quadruplexes in the frames. One of the main advantages of DNA origami is that one is able to incorporate various components (molecules or nanoparticles) in precise nanometric distances from each other.

5 Conclusion

In this master's thesis, I focused on the application of DNA origami in medicine. Specifically, I explored DNA origami nanostructures for targeted drug delivery or as sensors. Both fields are closely related to each other and are important for treatment and diagnostics. For targeted drug delivery, it is important to undertake experiments to see if the drug can be loaded into the nanostructure and then test them for their cytotoxicity against cancer cells. For sensing, it is important to undertake experiments to see if the nanostructure is stable after light irradiation as well as explore its functionalization by sensing molecules.

In the theoretical part of the work, I familiarized myself with various methods of preparing DNA origami nanostructures. This inspired me, on the one hand, to explore various types of drugs that can be used in chemotherapy and on the other hand, investigate properties of DNA origami for sensing.

The experimental part of the work consisted of two parts. The main goal of the first part was to optimize the method of the DNA origami preparation, drug loading (cisplatin and ruthenium complex) and to test their toxicity on the FaDu cancer cell line. For these experiments, I chose 3D DNA origami nanoblocks. During the preparation of pure DNA origami nanoblocks and drug-loaded DNA origami nanoblocks, I analyzed the influence of various parameters on the quality, stability and deposition of the nanostructures. The three-dimensional nanostructures are expected to be more stable in the biological environment although this might not be the case since we have observed some problems with the agglomeration both in buffers and cell media. I loaded cisplatin and ruthenium complex onto these nanoblocks and compared their cytotoxic effects. I observed better cytotoxicity for cisplatin-containing nanoblocks due to the more cytotoxic nature of cisplatin compared to the Ru-complex and the problems with the solubility of Ru-complex-loaded nanoblocks which could have affected the latter's distribution and uptake in cells. In the future, I propose to explore tracking of cellular uptake by incorporation of fluorescent dyes to better explain these findings, improve the stability and minimize the aggregation of DNA nanostructures in cell media, and eventually test their applications *in vivo*.

The main goal of the second part was to check the stability of DNA origami after laser irradiation and to test the possibility of attaching sensing molecules to DNA origami. I have observed extreme stability of DNA origami in wavelengths

where DNA does not significantly absorb such as those above 300 nm. This can have some implications for their use, for example, in photothermal therapy where wavelengths in the visible regime are often used. I was also able to incorporate a G-quadruplex sequence into a DNA origami nanoframe for possible sensing applications in the future.

References

[1] ZEROLOVÁ, Agnes. *DNA origami nanostruktury pro studium radiosenzitizačního efektu nanočástic*. 2021. Available also from: https://dspace.tul.cz/handle/15240/160405. Bakalářská práce. Technická univerzita v Liberci, Fakulta mechatroniky, informatiky a mezioborových studií, Liberec.

[2] SACCÀ, Barbara and Christof M. NIEMEYER. DNA Origami: The Art of Folding DNA. *Angewandte Chemie International Edition*. 2012, vol. 51, no. 1, pp. 58–66. ISSN 14337851. Available from DOI: 10.1002/anie.201105846.

[3] ABBAS, Muhammad et al. A DNA-based nanocarrier for efficient cancer therapy. *Journal of Pharmaceutical Analysis*. 2021, vol. 11, no. 3, pp. 330–339. ISSN 20951779. Available from DOI: 10.1016/j.jpha.2020.03.005.

[4] UDOMPRASERT, Anuttara and Thaned KANGSAMAKSIN. DNA origami applications in cancer therapy. *Cancer Science*. 2017, vol. 108, no. 8, pp. 1535–1543. ISSN 1349-7006. Available from DOI: 10.1111/cas.13290.

[5] ZHANG, Chao et al. DNA–affibody nanoparticle delivery system for cisplatin-based breast cancer chemotherapy. *RSC Advances* [online]. 2019, vol. 9, no. 4, pp. 1982–1989 [visited on 2023-03-06]. ISSN 2046-2069. Available from DOI: 10.1039/C8RA08735K.

[6] KUMAR, Vinit et al. DNA Nanotechnology for Cancer Therapeutics. *Theranostics*. 2016, vol. 6, no. 5, pp. 710–725. ISSN 1838-7640. Available from DOI: 10.7150/thno.14203.

[7] CHANDRASEKARAN, Arun Richard. Nuclease resistance of DNA nanostructures. *Nature Reviews Chemistry*. 2021, vol. 5, no. 4, pp. 225–239. ISSN 2397-3358. Available from DOI: 10.1038/s41570-021-00251-y.

[8] LACROIX, Aurélie and Hanadi F. SLEIMAN. DNA Nanostructures: Current Challenges and Opportunities for Cellular Delivery. *ACS Nano*. 2021, vol. 15, no. 3, pp. 3631–3645. ISSN 1936-0851, ISSN 1936-086X. Available from DOI: 10.1021/acsnano.0c06136.

[9] NANGREAVE, Jeanette et al. DNA origami: a history and current perspective. *Current Opinion in Chemical Biology*. 2010, vol. 14, no. 5, pp. 608–615. ISSN 13675931. Available from DOI: 10.1016/j.cbpa.2010.06.182.

[10] FAN, Chunhai and Qian LI. Advances in DNA Nanotechnology. *Small*. 2019, vol. 15, no. 26, p. 1902586. ISSN 1613-6810, ISSN 1613-6829. Available from DOI: 10.1002/smll.201902586.

[11] CHANDRASEKARAN, Arun Richard et al. Beyond the Fold: Emerging Biological Applications of DNA Origami. *ChemBioChem*. 2016, vol. 17, no. 12, pp. 1081–1089. ISSN 14394227. Available from DOI: 10.1002/cbic.201600038.

[12] SEEMAN, Nadrian C. Nucleic acid junctions and lattices. *Journal of Theoretical Biology*. 1982, vol. 99, no. 2, pp. 237–247. ISSN 00225193. Available from DOI: 10.1016/0022-5193(82)90002-9.

[13] JIANG, Wenjing et al. Recent Advances of DNA Origami Technology and Its Application in Nanomaterial Preparation. *Small Structures*. 2023, p. 2200376. ISSN 2688-4062, ISSN 2688-4062. Available from DOI: 10.1002/sstr.202200376.

[14] ROTHEMUND, Paul W. K. Folding DNA to create nanoscale shapes and patterns. *Nature*. 2006, vol. 440, no. 7082, pp. 297–302. ISSN 0028-0836, ISSN 1476-4687. Available from DOI: 10.1038/nature04586.

[15] EDWARDS, Angela and Hao YAN. DNA Origami. In: KJEMS, Jørgen, FERAPONTOVA, Elena, and GOTHELF, Kurt V. (eds.). *Nucleic Acid Nanotechnology*. Berlin, Heidelberg: Springer Berlin Heidelberg, 2014, vol. 29, pp. 93–133. ISBN 9783642388149 9783642388156. Available from DOI: 10.1007/978-3-642-38815-6_5.

[16] HONG, Fan et al. DNA Origami: Scaffolds for Creating Higher Order Structures. *Chemical Reviews*. 2017, vol. 117, no. 20, pp. 12584–12640. ISSN 0009-2665, ISSN 1520-6890. Available from DOI: 10.1021/acs.chemrev.6b00825.

[17] ROTHEMUND, Paul W. K. Scaffolded DNA Origami: from Generalized Multicrossovers to Polygonal Networks. In: CHEN, Junghuei, JONOSKA, Nataša, and ROZENBERG, Grzegorz (eds.). *Nanotechnology: Science and Computation*. Berlin/Heidelberg: Springer-Verlag, 2006, pp. 3–21. ISBN 9783540302957. Available from DOI: 10.1007/3-540-30296-4_1.

[18] ZENG, Jie et al. Self-Assembly of Microparticles by Supramolecular Homopolymerization of One Component DNA Molecule. *Small*. 2019, vol. 15, no. 26, p. 1805552. ISSN 1613-6810, ISSN 1613-6829. Available from DOI: 10.1002/smll.201805552.

[19] KELLER, Adrian et al. Probing Electron-Induced Bond Cleavage at the Single-Molecule Level Using DNA Origami Templates. *ACS Nano*. 2012, vol. 6, no. 5, pp. 4392–4399. ISSN 1936-0851, ISSN 1936-086X. Available from DOI: 10.1021/nn3010747.

[20] HAN, Dongran et al. DNA Origami with Complex Curvatures in Three-Dimensional Space. *Science*. 2011, vol. 332, no. 6027, pp. 342–346. ISSN 0036-8075, ISSN 1095-9203. Available from DOI: 10.1126/science.1202998.

[21] KICK, Benjamin et al. Efficient Production of Single-Stranded Phage DNA as Scaffolds for DNA Origami. *Nano Letters*. 2015, vol. 15, no. 7, pp. 4672–4676. ISSN 1530-6984, ISSN 1530-6992. Available from DOI: 10.1021/acs.nanolett.5b01461.

[22] NICKELS, Philipp C. et al. DNA Origami Structures Directly Assembled from Intact Bacteriophages. *Small*. 2014, vol. 10, no. 9, pp. 1765–1769. ISSN 16136810. Available from DOI: 10.1002/smll.201303442.

[23] MARCHI, Alexandria N. et al. Toward Larger DNA Origami. *Nano Letters*. 2014, vol. 14, no. 10, pp. 5740–5747. ISSN 1530-6984, ISSN 1530-6992. Available from DOI: 10.1021/nl502626s.

[24] SAID, Hassan et al. M1.3 – a small scaffold for DNA origami. *Nanoscale*. 2013, vol. 5, no. 1, pp. 284–290. ISSN 2040-3364, ISSN 2040-3372. Available from DOI: 10.1039/C2NR32393A.

[25] YANG, Yang et al. DNA Origami with Double-Stranded DNA As a Unified Scaffold. *ACS Nano*. 2012, vol. 6, no. 9, pp. 8209–8215. ISSN 1936-0851, ISSN 1936-086X. Available from DOI: 10.1021/nn302896c.

[26] LIU, Xiaoguo et al. Complex silica composite nanomaterials templated with DNA origami. *Nature*. 2018, vol. 559, no. 7715, pp. 593–598. ISSN 0028-0836, ISSN 1476-4687. Available from DOI: 10.1038/s41586-018-0332-7.

[27] AGARWAL, Nayan P. et al. Structural Transformation of Wireframe DNA Origami *via* DNA Polymerase Assisted Gap-Filling. *ACS Nano*. 2018, vol. 12, no. 3, pp. 2546–2553. ISSN 1936-0851, ISSN 1936-086X. Available from DOI: 10.1021/acsnano.7b08345.

[28] ZHANG, Fei et al. Complex wireframe DNA origami nanostructures with multi-arm junction vertices. *Nature Nanotechnology*. 2015, vol. 10, no. 9, pp. 779–784. ISSN 1748-3387, ISSN 1748-3395. Available from DOI: 10.1038/nnano.2015.162.

[29] CHEN, Junghuei and Nadrian C. SEEMAN. Synthesis from DNA of a molecule with the connectivity of a cube. *Nature*. 1991, vol. 350, no. 6319, pp. 631–633. ISSN 0028-0836, ISSN 1476-4687. Available from DOI: 10.1038/350631a0.

[30] SHIH, William M., Joel D. QUISPE, and Gerald F. JOYCE. A 1.7-kilobase single-stranded DNA that folds into a nanoscale octahedron. *Nature*. 2004, vol. 427, no. 6975, pp. 618–621. ISSN 0028-0836, ISSN 1476-4687. Available from DOI: 10.1038/nature02307.

[31] ENDO, Masayuki et al. DNA Prism Structures Constructed by Folding of Multiple Rectangular Arms. *Journal of the American Chemical Society*. 2009, vol. 131, no. 43, pp. 15570–15571. ISSN 0002-7863, ISSN 1520-5126. Available from DOI: 10.1021/ja904252e.

[32] KUZUYA, Akinori and Makoto KOMIYAMA. Design and construction of a box-shaped 3D-DNA origami. *Chemical Communications*. 2009, no. 28, p. 4182. ISSN 1359-7345, ISSN 1364-548X. Available from DOI: 10.1039/b907800b.

[33] HAN, Dongran et al. Folding and cutting DNA into reconfigurable topological nanostructures. *Nature Nanotechnology*. 2010, vol. 5, no. 10, pp. 712–717. ISSN 1748-3387, ISSN 1748-3395. Available from DOI: 10.1038/nnano.2010.193.

[34] SMITH, David M. et al. A Structurally Variable Hinged Tetrahedron Framework from DNA Origami. *Journal of Nucleic Acids*. 2011, vol. 2011, pp. 1–9. ISSN 2090-021X. Available from DOI: 10.4061/2011/360954.

[35] OUYANG, Xiangyuan et al. Docking of Antibodies into the Cavities of DNA Origami Structures. *Angewandte Chemie International Edition*. 2017, vol. 56, no. 46, pp. 14423–14427. ISSN 14337851. Available from DOI: 10.1002/anie.201706765.

[36] TIGGES, Thomas et al. 3D DNA Origami Cuboids as Monodisperse Patchy Nanoparticles for Switchable Hierarchical Self-Assembly. *Nano Letters*. 2016, vol. 16, no. 12, pp. 7870–7874. ISSN 1530-6984, ISSN 1530-6992. Available from DOI: 10.1021/acs.nanolett.6b04146.

[37] IJÄS, Heini et al. Reconfigurable DNA Origami Nanocapsule for pH-Controlled Encapsulation and Display of Cargo. *ACS Nano*. 2019, vol. 13, no. 5, pp. 5959–5967. ISSN 1936-0851, ISSN 1936-086X. Available from DOI: 10.1021/acsnano.9b01857.

[38] WAGENBAUER, Klaus F., Christian SIGL, and Hendrik DIETZ. Gigadalton-scale shape-programmable DNA assemblies. *Nature*. 2017, vol. 552, no. 7683, pp. 78–83. ISSN 0028-0836, ISSN 1476-4687. Available from DOI: 10.1038/nature24651.

[39] DOUGLAS, Shawn M. et al. Rapid prototyping of 3D DNA-origami shapes with caDNAno. *Nucleic Acids Research*. 2009, vol. 37, no. 15, pp. 5001–5006. ISSN 1362-4962, ISSN 0305-1048. Available from DOI: 10.1093/nar/gkp436.

[40] WANG, Pengfei et al. The Beauty and Utility of DNA Origami. *Chem*. 2017, vol. 2, no. 3, pp. 359–382. ISSN 24519294. Available from DOI: 10.1016/j.chempr.2017.02.009.

[41] DEEPA, Kannan, Siddhartha SINGHA, and Tapobrata PANDA. Doxorubicin Nanoconjugates. *Journal of Nanoscience and Nanotechnology*. 2014, vol. 14, no. 1, pp. 892–904. ISSN 15334880, ISSN 15334899. Available from DOI: 10.1166/jnn.2014.8765.

[42] ABRAHAM, Sheela A. et al. The Liposomal Formulation of Doxorubicin. In: *Methods in Enzymology*. Elsevier, 2005, vol. 391, pp. 71–97. ISBN 9780121827960. Available from DOI: 10.1016/S0076-6879(05)91004-5.

[43] MINOTTI, Giorgio et al. Anthracyclines: Molecular Advances and Pharmacologic Developments in Antitumor Activity and Cardiotoxicity. *Pharmacological Reviews*. 2004, vol. 56, no. 2, pp. 185–229. ISSN 0031-6997, ISSN 1521-0081. Available from DOI: 10.1124/pr.56.2.6.

[44] RIVANKAR, Sangeeta. An overview of doxorubicin formulations in cancer therapy. *Journal of Cancer Research and Therapeutics*. 2014, vol. 10, no. 4, p. 853. ISSN 0973-1482. Available from DOI: 10.4103/0973-1482.139267.

[45] CARVALHO, Cristina et al. Doxorubicin: The Good, the Bad and the Ugly Effect. *Current Medicinal Chemistry*. [N.d.], vol. 16, no. 25, pp. 3267–3285. Available from DOI: 10.2174/092986709788803312.

[46] PAN, Qingshan et al. Aptamer-Functionalized DNA Origami for Targeted Codelivery of Antisense Oligonucleotides and Doxorubicin to Enhance Therapy in Drug-Resistant Cancer Cells. *ACS Applied Materials & Interfaces*. 2020, vol. 12, no. 1, pp. 400–409. ISSN 1944-8244, ISSN 1944-8252. Available from DOI: 10.1021/acsami.9b20707.

[47] PATEL, Anand G and Scott H KAUFMANN. How does doxorubicin work? *eLife*. 2012, vol. 1, e00387. ISSN 2050-084X. Available from DOI: 10.7554/eLife.00387.

[48] ZHAO, Na, Martin C WOODLE, and A. James MIXSON. Advances in Delivery Systems for Doxorubicin. *Journal of Nanomedicine & Nanotechnology*. 2018, vol. 09, no. 05. ISSN 21577439. Available from DOI: 10.4172/2157-7439.1000519.

[49] AGUDELO, Daniel et al. Intercalation of antitumor drug doxorubicin and its analogue by DNA duplex: Structural features and biological implications. *International Journal of Biological Macromolecules*. 2014, vol. 66, pp. 144–150. ISSN 01418130. Available from DOI: 10.1016/j.ijbiomac.2014.02.028.

[50] TACAR, Oktay, Pornsak SRIAMORNSAK, and Crispin R DASS. Doxorubicin: an update on anticancer molecular action, toxicity and novel drug delivery systems. *Journal of Pharmacy and Pharmacology*. 2012, vol. 65, no. 2, pp. 157–170. ISSN 2042-7158, ISSN 0022-3573. Available from DOI: 10.1111/j.2042-7158.2012.01567.x.

[51] ZENG, Yun et al. Time-lapse live cell imaging to monitor doxorubicin release from DNA origami nanostructures. *Journal of Materials Chemistry B*. 2018, vol. 6, no. 11, pp. 1605–1612. ISSN 2050-750X, ISSN 2050-7518. Available from DOI: 10.1039/C7TB03223D.

[52] ALDOSSARY, S. Review on Pharmacology of Cisplatin: Clinical Use, Toxicity and Mechanism of Resistance of Cisplatin. *Biomedical and Pharmacology Journal*. 2019, vol. 12, no. 1, pp. 7–15. Available from DOI: 10.13005/bpj/1608.

[53] DASARI, S. and P. B. TCHOUNWOU. Cisplatin in cancer therapy: Molecular mechanisms of action. *European Journal of Pharmacology*. 2014, vol. 740, pp. 364–378. ISSN 0014-2999. Available from DOI: 10.1016/j.ejphar.2014.07.025.

[54] LOSKOTOVÁ, H. and V. BRABEC. DNA interactions of cisplatin tethered to the DNA minor groove binder distamycin. *European Journal of Biochemistry*. 1999, vol. 266, no. 2, pp. 392–402. ISSN 0014-2956. Available from DOI: 10.1046/j.1432-1327.1999.00866.x.

[55] MANTRI, Yogita, Stephen J. LIPPARD, and Mu-Hyun BAIK. Bifunctional Binding of Cisplatin to DNA: Why Does Cisplatin Form 1,2-Intrastrand Cross-Links with AG But Not with GA? *Journal of the American Chemical Society*. 2007, vol. 129, no. 16, pp. 5023–5030. ISSN 0002-7863, ISSN 1520-5126. Available from DOI: 10.1021/ja067631z.

[56] ROSENBERG, Barnett, Loretta VAN CAMP, and Thomas KRIGAS. Inhibition of Cell Division in Escherichia coli by Electrolysis Products from a Platinum Electrode. *Nature*. 1965, vol. 205, no. 4972, pp. 698–699. ISSN 0028-0836, ISSN 1476-4687. Available from DOI: 10.1038/205698a0.

[57] WANG, Yaping et al. Doxorubicin/cisplatin co-loaded hyaluronic acid/chitosan-based nanoparticles for in vitro synergistic combination chemotherapy of breast cancer. *Carbohydrate Polymers*. 2019, vol. 225, p. 115206. ISSN 01448617. Available from DOI: 10.1016/j.carbpol.2019.115206.

[58] SZTURZ, Petr et al. Weekly Low-Dose Versus Three-Weekly High-Dose Cisplatin for Concurrent Chemoradiation in Locoregionally Advanced Non-Nasopharyngeal Head and Neck Cancer: A Systematic Review and Meta-Analysis of Aggregate Data. *The Oncologist*. 2017, vol. 22, no. 9, pp. 1056–1066. ISSN 1083-7159, ISSN 1549-490X. Available from DOI: 10 . 1634 / theoncologist.2017-0015.

[59] IWATA, Hiromitsu et al. Combined effects of cisplatin and photon or proton irradiation in cultured cells: radiosensitization, patterns of cell death and cell cycle distribution. *Journal of Radiation Research*. 2020, vol. 61, no. 6, pp. 832–841. ISSN 0449-3060, ISSN 1349-9157. Available from DOI: 10.1093/jrr/rraa065.

[60] YANG, Hua, Kimberly L. METERA, and Hanadi F. SLEIMAN. DNA modified with metal complexes: Applications in the construction of higher order metal–DNA nanostructures. *Coordination Chemistry Reviews*. 2010, vol. 254, no. 19-20, pp. 2403–2415. ISSN 00108545. Available from DOI: 10.1016/j.ccr.2010.02.026.

[61] ROCHA, Clarissa Ribeiro Reily et al. DNA repair pathways and cisplatin resistance: an intimate relationship. *Clinics*. 2018, vol. 73, e478s. ISSN 18075932. Available from DOI: 10.6061/clinics/2018/e478s.

[62] BRABEC, Viktor, Ondrej HRABINA, and Jana KASPARKOVA. Cytotoxic platinum coordination compounds. DNA binding agents. *Coordination Chemistry Reviews*. 2017, vol. 351, pp. 2–31. ISSN 00108545. Available from DOI: 10.1016/j.ccr.2017.04.013.

[63] PAPROCKA, Renata et al. Latest developments in metal complexes as anticancer agents. *Coordination Chemistry Reviews*. 2022, vol. 452, p. 214307. ISSN 00108545. Available from DOI: 10.1016/j.ccr.2021.214307.

[64] GU, Yun-Qiong et al. Ru(III) complexes with pyrazolopyrimidines as anticancer agents: bioactivities and the underlying mechanisms. *Dalton Transactions*. 2022, vol. 51, no. 4, pp. 1333–1343. ISSN 1477-9226, ISSN 1477-9234. Available from DOI: 10.1039/D1DT02765D.

[65] SCHATZSCHNEIDER, Ulrich et al. Cellular Uptake, Cytotoxicity, and Metabolic Profiling of Human Cancer Cells Treated with Ruthenium(II) Polypyridyl Complexes [Ru(bpy)$_2$(N-N)]Cl$_2$ with N-N=bpy, phen, dpq, dppz, and dppn. *ChemMedChem* [online]. 2008, vol. 3, no. 7, pp. 1104–1109 [visited on 2023-05-09]. ISSN 18607179, ISSN 18607187. Available from DOI: 10.1002/cmdc.200800039.

[66] KANAOUJIYA, Rahul et al. Ruthenium Based Anticancer Compounds and Their Importance. *Journal of scientific research*. 2020, vol. 64, no. 01, pp. 264–268. ISSN 04479483. Available from DOI: 10.37398/JSR.2020.640150.

[67] LEE, Sang Yeul, Chul Young KIM, and Tae-Gyu NAM. Ruthenium Complexes as Anticancer Agents: A Brief History and Perspectives. *Drug Design, Development and Therapy*. 2020, vol. 14, pp. 5375–5392. Available from DOI: 10.2147/DDDT.S275007.

[68] CARDIN, Christine J., John M. KELLY, and Susan J. QUINN. Photochemically active DNA-intercalating ruthenium and related complexes – insights by combining crystallography and transient spectroscopy. *Chemical Science*. 2017, vol. 8, no. 7, pp. 4705–4723. ISSN 2041-6520, ISSN 2041-6539. Available from DOI: 10.1039/C7SC01070B.

[69] DE LA CADENA, Alejandro et al. Ultrafast in cellulo photoinduced dynamics processes of the paradigm molecular light switch [Ru(bpy)2dppz]2+. *Scientific Reports*. 2016, vol. 6, no. 1, p. 33547. ISSN 2045-2322. Available from DOI: 10.1038/srep33547.

[70] ZHANG, Qian, Qiao JIANG, and Na a spol. LI. DNA Origami as an *In Vivo* Drug Delivery Vehicle for Cancer Therapy. *ACS Nano*. 2014, vol. 8, no. 7, pp. 6633–6643. ISSN 1936-0851, ISSN 1936-086X. Available from DOI: 10.1021/nn502058j.

[71] JIANG, Qiao et al. Rationally Designed DNA-Origami Nanomaterials for Drug Delivery In Vivo. *Advanced Materials*. 2019, vol. 31, no. 45, p. 1804785. ISSN 0935-9648, ISSN 1521-4095. Available from DOI: 10.1002/adma.201804785.

[72] HEGER, Zbyněk et al. Modern Nanomedicine in Treatment of Lung Carcinomas. *Klinicka onkologie*. 2015, vol. 28, no. 4, pp. 245–250. ISSN 0862495X, ISSN 18025307. Available from DOI: 10.14735/amko2015245.

[73] WILHELM, Stefan et al. Analysis of nanoparticle delivery to tumours. *Nature Reviews Materials*. 2016, vol. 1, no. 5, p. 16014. ISSN 2058-8437. Available from DOI: 10.1038/natrevmats.2016.14.

[74] PAL, Suchetan and Tatini RAKSHIT. Folate-Functionalized DNA Origami for Targeted Delivery of Doxorubicin to Triple-Negative Breast Cancer. *Frontiers in Chemistry*. 2021, vol. 9, p. 721105. ISSN 2296-2646. Available from DOI: 10.3389/fchem.2021.721105.

[75] ZHANG, Tao et al. Design, fabrication and applications of tetrahedral DNA nanostructure-based multifunctional complexes in drug delivery and biomedical treatment. *Nature Protocols*. 2020, vol. 15, no. 8, pp. 2728–2757. ISSN 1754-2189, ISSN 1750-2799. Available from DOI: 10.1038/s41596-020-0355-z.

[76] MA, Wenjuan et al. Biomimetic Nanoerythrosome-Coated Aptamer–DNA Tetrahedron/Maytansine Conjugates: pH-Responsive and Targeted Cytotoxicity for HER2-Positive Breast Cancer. *Advanced Materials*. 2022, vol. 34, no. 46, p. 2109609. ISSN 0935-9648, ISSN 1521-4095. Available from DOI: 10.1002/adma.202109609.

[77] SALA, Leo et al. Cisplatin-Cross-Linked DNA Origami Nanostructures for Drug Delivery Applications. *ACS Applied Nano Materials*. 2022, vol. 5, no. 9, pp. 13267–13275. ISSN 2574-0970, ISSN 2574-0970. Available from DOI: 10.1021/acsanm.2c02976.

[78] WEIDEN, Jorieke and Maartje M.C. BASTINGS. DNA origami nanostructures for controlled therapeutic drug delivery. *Current Opinion in Colloid & Interface Science*. 2021, vol. 52, p. 101411. ISSN 13590294. Available from DOI: 10.1016/j.cocis.2020.101411.

[79] ZHONG, Yi-Fang et al. DNA Nanostructures as Pt(IV) Prodrug Delivery Systems to Combat Chemoresistance. *Small*. 2020, vol. 16, no. 38, p. 2003646. ISSN 1613-6810, ISSN 1613-6829. Available from DOI: 10.1002/smll.202003646.

[80] YANG, Hualin, Yu ZHOU, and Juewen LIU. G-quadruplex DNA for construction of biosensors. *TrAC Trends in Analytical Chemistry*. 2020, vol. 132, p. 116060. ISSN 01659936. Available from DOI: 10.1016/j.trac.2020.116060.

[81] LIU, Qiaoling et al. Aptamer-conjugated nanomaterials for specific cancer cell recognition and targeted cancer therapy. *NPG Asia Materials*. 2014, vol. 6, no. 4, e95–e95. ISSN 1884-4049, ISSN 1884-4057. Available from DOI: 10.1038/am.2014.12.

[82] KOTKOWIAK, Weronika et al. Improved RE31 Analogues Containing Modified Nucleic Acid Monomers: Thermodynamic, Structural, and Biological Effects. *Journal of Medicinal Chemistry*. 2019, vol. 62, no. 5, pp. 2499–2507. ISSN 0022-2623, ISSN 1520-4804. Available from DOI: 10.1021/acs.jmedchem.8b01806.

[83] SHEN, Luyao, Pengfei WANG, and Yonggang KE. DNA Nanotechnology-Based Biosensors and Therapeutics. *Advanced Healthcare Materials*. 2021, vol. 10, no. 15, p. 2002205. ISSN 2192-2640, ISSN 2192-2659. Available from DOI: 10.1002/adhm.202002205.

[84] RAVEENDRAN, Mukhil et al. Rational design of DNA nanostructures for single molecule biosensing. *Nature Communications*. 2020, vol. 11, no. 1, p. 4384. ISSN 2041-1723. Available from DOI: 10.1038/s41467-020-18132-1.

[85] KE, Yonggang et al. Self-Assembled Water-Soluble Nucleic Acid Probe Tiles for Label-Free RNA Hybridization Assays. *Science*. 2008, vol. 319, no. 5860, pp. 180–183. ISSN 0036-8075, ISSN 1095-9203. Available from DOI: 10.1126/science.1150082.

[86] BEJ, Asim K., Meena H. MAHBUBANI, and Ronald M. ATLAS. Amplification of Nucleic Acids by Polymerase Chain Reaction (PCR) and Other Methods and their Applications. *Critical Reviews in Biochemistry and Molecular Biology*. 1991, vol. 26, no. 3-4, pp. 301–334. ISSN 1040-9238, ISSN 1549-7798. Available from DOI: 10.3109/10409239109114071.

[87] PENG, Hanyong et al. Signal Amplification in Living Cells: A Review of microRNA Detection and Imaging. *Analytical Chemistry*. 2020, vol. 92, no. 1, pp. 292–308. ISSN 0003-2700, ISSN 1520-6882. Available from DOI: 10.1021/acs.analchem.9b04752.

[88] NIE, Wenyan et al. Low-Fouling Surface Plasmon Resonance Sensor for Highly Sensitive Detection of MicroRNA in a Complex Matrix Based on the DNA Tetrahedron. *Analytical Chemistry*. 2018, vol. 90, no. 21, pp. 12584–12591. ISSN 0003-2700, ISSN 1520-6882. Available from DOI: 10.1021/acs.analchem.8b02686.

[89] LI, Yuqing and Juewen LIU. Aptamer-based strategies for recognizing adenine, adenosine, ATP and related compounds. *The Analyst*. 2020, vol. 145, no. 21, pp. 6753–6768. ISSN 0003-2654, ISSN 1364-5528. Available from DOI: 10.1039/D0AN00886A.

[90] HUANG, Rongrong, Nongyue HE, and Zhiyang LI. Recent progresses in DNA nanostructure-based biosensors for detection of tumor markers. *Biosensors and Bioelectronics*. 2018, vol. 109, pp. 27–34. ISSN 09565663. Available from DOI: 10.1016/j.bios.2018.02.053.

[91] KUZUYA, Akinori et al. Nanomechanical DNA origami 'single-molecule beacons' directly imaged by atomic force microscopy. *Nature Communications*. 2011, vol. 2, no. 1, p. 449. ISSN 2041-1723. Available from DOI: 10.1038/ncomms1452.

[92] ENDO, Masayuki et al. Single-Molecule Manipulation of the Duplex Formation and Dissociation at the G-Quadruplex/i-Motif Site in the DNA Nanostructure. *ACS Nano*. 2015, vol. 9, no. 10, pp. 9922–9929. ISSN 1936-0851, ISSN 1936-086X. Available from DOI: 10.1021/acsnano.5b03413.

[93] ENDO, Masayuki et al. Regulation of DNA Methylation Using Different Tensions of Double Strands Constructed in a Defined DNA Nanostructure. *Journal of the American Chemical Society*. 2010, vol. 132, no. 5, pp. 1592–1597. ISSN 0002-7863, ISSN 1520-5126. Available from DOI: 10.1021/ja907649w.

[94] ENDO, Masayuki, Yangyang YANG, and Hiroshi SUGIYAMA. DNA origami technology for biomaterials applications. *Biomater. Sci.* 2013, vol. 1, no. 4, pp. 347–360. ISSN 2047-4830, ISSN 2047-4849. Available from DOI: 10.1039/C2BM00154C.

[95] LI, Hailong et al. G-quadruplex-based ultrasensitive and selective detection of histidine and cysteine. *Biosensors and Bioelectronics*. 2013, vol. 41, pp. 563–568. ISSN 09565663. Available from DOI: 10.1016/j.bios.2012.09.024.

[96] QIN, Haixia et al. G-Quadruplex-Modulated Fluorescence Detection of Potassium in the Presence of a 3500-Fold Excess of Sodium Ions. *Analytical Chemistry*. 2010, vol. 82, no. 19, pp. 8356–8360. ISSN 0003-2700, ISSN 1520-6882. Available from DOI: 10.1021/ac101894b.

[97] SALA, Leo et al. Different Mechanisms of DNA Radiosensitization by 8-Bromoadenosine and 2 -Deoxy-2 -fluorocytidine Observed on DNA Origami Nanoframe Supports. *The Journal of Physical Chemistry Letters*. 2022, vol. 13, no. 17, pp. 3922–3928. ISSN 1948-7185, ISSN 1948-7185. Available from DOI: 10.1021/acs.jpclett.2c00584.

[98] CERVINKA, Jakub et al. Ruthenium(II)–Tris-pyrazolylmethane Complexes Inhibit Cancer Cell Growth by Disrupting Mitochondrial Calcium Homeostasis. *Journal of Medicinal Chemistry*. 2022, vol. 65, no. 15, pp. 10567–10587. ISSN 0022-2623, ISSN 1520-4804. Available from DOI: 10.1021/acs.jmedchem.2c00722.

[99] OLEJKO, L., P. J. CYWIŃSKI, and I. BALD. An ion-controlled four-color fluorescent telomeric switch on DNA origami structures. *Nanoscale*. 2016, vol. 8, no. 19, pp. 10339–10347. ISSN 2040-3364, ISSN 2040-3372. Available from DOI: 10.1039/C6NR00119J.

[100] KOGIKOSKI, Sergio et al. Raman Enhancement of Nanoparticle Dimers Self-Assembled Using DNA Origami Nanotriangles. *Molecules*. 2021, vol. 26, no. 6, p. 1684. ISSN 1420-3049. Available from DOI: 10.3390/molecules26061684.

List of Figures